Title
SCALING AND NON-SCALING OF INCLUSIVE PION PRODUCTION IN NUCLEAR COLLISIONS

Author
Landau, R.H.

Publication Date
1978-04-01

Submitted to Physical Review C

LBL-7719
Preprint

SCALING AND NON-SCALING OF INCLUSIVE PION PRODUCTION IN NUCLEAR COLLISIONS

R. H. Landau and M. Gyulassy

April 1978

Prepared for the U. S. Department of Energy
under Contract W-7405-ENG-48

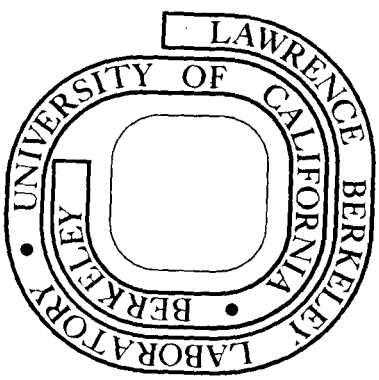

LBL-7719

DISCLAIMER

SCALING AND NON-SCALING OF INCLUSIVE PION PRODUCTION IN NUCLEAR COLLISIONS*

R. H. Landau† and M. Gyulassy
Nuclear Science Division

Lawrence Berkeley Laboratory
University of California
Berkeley, California 94720

April 1978

ABSTRACT

An examination is made of the degree of scaling observed in inclusive pion production from high energy nuclear collisions. While apparent scaling does occur for forward pion production, the scaling limit is not reached in backward π production between 0.7 - 8 GeV/nucleon. We show that the shapes of the pion inclusive cross sections in both the forward and backward directions can be explained by a simple, hard scattering model employing elementary proton-proton π production rates, or alternatively, in terms of elementary proton-light cluster π production rates. The essential features of this model are an invariant parametization of the elementary subprocess, the proper handling of kinetmatical effects, and the use of a universal pseudo-Fermi motion distribution function with an exponential tail for nucleons or clusters. We find that much of the "apparent" scaling in the forward direction can be attributed to kinematical effects. The importance of final state interactions on the interpretation of the pseudo-Fermi function is emphasized, and the

*This work was done with support from the U. S. Department of Energy.
†On leave from Oregon State University.

connection to quasi-two-body scaling is examined.

PAC: 24.50. + g, 25.10. + s, 25.40Rb, 25.50.-n, 25.60-t, 25.70. - z

#

KEYWORDS:

NUCLEAR REACTIONS Cu(p,π)X, p(p,π)X, D(p,π)X, Cu(α,π)X, C(p,π)X, C(d,π)X, C(α,π)X, 0.7 < E < 8 GeV/nucl.

Scaling of invariant cross sections, Feynman scaling variable, hard scattering models, large momentum behavior of single particle momentum distributions, pion production, clustering.

I. INTRODUCTION

Data on nuclear collisions are now becoming available[1-6] for a wide variety of projectile (P = p,d,α,C) and target (T = p,···,U) combinations in the energy range from ~ 500 MeV to ~ 10 GeV per projectile nucleon. Of particular current interest[7-13] is the observation of pion and proton fragments with momenta larger than those obtainable in elementary nucleon-nucleon scattering at these same energies. Such fragments can arise only as a result of the coherent interaction of many nucleons and Fermi motion, i.e. nuclear binding effects. The hope therefore is that by studying the highest energy single particle fragments, the cluster aspects of nuclei and/or the high momentum tail of nuclear wavefunctions can be deduced.

Recently, Schmidt and Blankenbeder (SB)[9] have proposed a hard scattering model in which the x_F (Feynman scaling variable) dependence of the inclusive cross sections provides information on that high momentum component of nuclear wavefunctions. One very attractive feature of the SB model is that it yields simple counting rues which predict a power law behavior of cross sections as $d\sigma \sim (1-x_F)^S$. In applications to π and p production in the projectile fragmentation region ($\theta_{lab} \approx 0$ and $P << T$) the model enjoyed considerable success in reproducing widely varying powers S ($3 \lesssim S \lesssim 65$). Our study is motivated by those successes and the subsequent questions raised[6,10] concerning the predictions of the model for π production in the target fragmentation region ($\theta_{lab} \approx 180°$).

We display below the discovery of Chessin et al.[6] that for the energies studied (1 - 8 BeV) the scaling limit has not yet been attained in backward π production. In addition, the rate of fall off with x_F is much less than predicted in the SB model, suggesting a possible cluster production mechanism.[10] We then attempt to modify the SB model in the spirit of the static cluster models of Ref. (11). While improving the fit, large descrepancies still remain. Finally, we are led to introduce a pseudo-probability distribution, $\rho(\tilde{p})$, to account for Fermi motion of the clusters in the spirit of Refs. (12,13). For "clusters" consisting of a single nucleon, our $\rho(\tilde{p})$ is similar to that of Amado and Woloshyn[7,14,15] and Frankel.[8,23]

With $\rho(\tilde{p})$ in the hard scattering model, we can account for both the magnitude and the energy dependence (non-scaling) of the power S controlling the fall-off of the backward π production in terms of either π production off light clusters or production off protons.

We next investigate why apparent scaling exists in the projectile fragmentation region but not in the target fragmentation region. We show that forward angle production is mainly sensitive to proper kinematics but not to the dynamical details of the model. In fact, the shapes of the pion inclusive cross sections in the forward region can be explained in terms of nucleon-cluster scattering with any size cluster $c = 1$ to A_T. In particular, simple nucleon-nucleon scattering including the same pseudo-Fermi distribution as used for the target fragmentation region can account for the data in the projectile fragmentation region as $x_F \to 1$.

Thus, π production in both the projectile and target fragmentation regions can be understood in terms of a rather transparent, simple model. Previous indications[11,12] had led us to believe that at least in the target fragmentation region such a simple model could not account for the data.

We also analyze the connection between our $\rho(\tilde{p})$ and the distribution function considered in Refs. (7,8). We conclude, as in Ref. (14), that final state interactions cloud the interpretation of both distributions. In particular, neither distribution can be interpreted as the true probability of finding a nucleon with momentum p inside a nucleus. Nevertheless, they have the great virtue of reducing a wealth of seemingly unrelated data to one simple function. A corollary of the above is that much of the differences between reactions producing high energy pions can be traced to simple kinematic (Lorentz transformation) effects. Thus, while experiments of this sort provide information on $\rho(\tilde{p})$, more theoretical work is needed on the structure and reactive content of this function.

II. HARD SCATTERING MODELS

We consider in this paper hard scattering (or impulse approximation) models[7-13] (HSM) that have had much success in reproducing the high energy particle production inclusive cross sections in proton and heavy ion induced reactions. For the proton case the invariant single pion inclusive cross section

$$R(p + A \to \pi + X) = E_\pi \frac{d\sigma}{d^3p_\pi} = \frac{E_\pi}{p^2_\pi} \frac{d\sigma}{d\Omega dp_\pi} \tag{1}$$

is computed in HSM from known $R(p + p \to \pi + x)$ data. Of course, the actual scattering amplitude $\mathcal{M}(p + A \to \pi + X)$ is, as illustrated in Fig. Ia, very complex. The complications arise from three unknown factors:

1) $\psi_A(p')$ = amplitude of finding an off-shell nucleon with four momentum p' in a nucleus with A nucleons.

2) $T_{pp'\pi x}$ = off-shell $p + p' \to \pi + x$ amplitude.

3) $\Omega_{\pi X}$ = final state distortion factor.

One of the major simplifying assumptions of the HSM is the neglect of final state interactions,

$$\Omega_{\pi X} = 1, \tag{2}$$

so that Fig. Ia reduces to Ib. The hope is that $\Omega_{\pi X}$ in Fig. Ia affects mainly the normalization and not the shape of R in eq. (1). The normalization of R is therefore not well determined in these models. As we discuss below, the price paid for eq. (2) is that final conclusions drawn in HSM, even if data are fit well, must be drawn with extra care.[14]

The second major assumption in HSM is how the off-shell amplitude, $T_{pp'\pi x}$, is evaluated. Experimentally, it is only known on-shell for certain energies. The common prescription is to evaluate the on-shell amplitude with the Mandelstam variables $s' = (p + p')^2$, $t' = -(k_\pi - p)^2$, $u' = -(k_\pi - p')^2$ by setting the energy of the virtual nucleon with momentum $\tilde{p}'$ to be $p'_o = \sqrt{p'^2 + m^2}$. Therefore,

$$T_{pp'\pi x} = T^{\text{on-shell}}_{pp'\pi x}(s',t',u'). \tag{3}$$

In eq. (3) we surpress the other kinematic variables associated with the final nucleons. Of course, eq. (3) cannot be justified a priori and can only be viewed as a prescription. In the absence of a detailed field theory it is, however, a reasonable guess. By adopting eqn. (2,3), the hard scattering models cease to be theories and become phenomenological tools to study the relative importance of particular physical effects such as kinematics or clustering on the data. It is as phenomenological tools that HSM are valuable models.

The final expression for R for proton projectiles is then

$$R(p + A \to \pi + X) = N_A \int \frac{d^3p'}{\varepsilon(p')} \; G_A(p') \; R(p + p \to \pi + x;\; s',t',u') \; \mathcal{P}, \tag{4}$$

where $G_A(p')$ is the pseudo probability of finding a nucleon with momentum p' in the target A CM (the lab here), and where $\mathcal{P}$ is a phase space factor involving the ratio of relative flux factors. In addition, the phase space factor $\mathcal{P}$ vanishes for those momenta p' that lead to pion produced in the subprocess that are outside the kinematic boundaries for pions produced in the $pA \to \pi X$ collision.

For nuclear projectiles, the expression for R becomes

$$R(B + A \to \pi + X) = N_{AB} \int \frac{d^3\tilde{p}'}{\varepsilon(\tilde{p}')} \frac{d^3\tilde{q}'}{\varepsilon(\tilde{q}')} G_A(\tilde{p}') G_B(\tilde{q}')$$

$$\times R(p + p \to \pi + x; s',t',u') \mathcal{P}, \quad (5)$$

where p' is the momentum of one nucleon in the A frame and q' is the momentum of the other in the B frame. The internal variables s',t',u' are then computed by transforming q' to the A frame and setting $s' = (p' + (q')_A)^2$ etc. The phase space factor $\mathcal{P}$ in eq. (5) also serves to limit the domain of the p',q' integrations so again only kinematically allowed pions are produced in the subprocess. Since the ratio of relative velocities in $\mathcal{P}$ is always near 1 for the relativistic collision we consider here, $\mathcal{P}$ is effectively a theta function constraint on the momenta in both eqs. (4,5). The normalization factors N_A and N_{AB} in eqs. (4,5) are not determined in the model we present.

We regard eqs. (4,5) as definitions of $G_A(\tilde{p})$, and call $G_A(\tilde{p})$ a pseudo-probability distribution to emphasize that G_A could be interpreted as the probability of finding a nucleon with momentum p inside a nucleus A only if eqs. (4,5) were exact.

Equations (4,5) are the basis of all hard scattering models. The main differences between those models[7-13] lie then in the specific choices of $G_A(p)$, the exact kinematical region where $\mathcal{P} \neq 0$, and the parameterization of the elementary $pp \to \pi x$ rates. In the next section, we consider first the particular model developed in Ref. (9).

III. THE SCHMIDT-BLANKENBECLER (SB) MODEL[9]

The remarkable property of the pion production rates observed[1] in the projectile fragmentation region is that although they vary over five orders of magnitude when plotted against the Feynman scaling variable x_F, they appear to be energy independent (i.e., scale) for $1 < T_p < 5$ GeV/nucleon. To account for this scaling SB proposed a version of the relativistic hard scattering model that is successful in understanding hadron-hadron interactions. We analyze some features of their model below.

For the inclusive (sub) process $b + a \rightarrow \pi + x$, where "b" nucleons with total 4-momentum p_b are incident on "a" nucleons with 4-momentum p_a producing pion π with 4-momentum p_π, and anything "x", the maximum allowed momentum of the pion in the ab center of mass occurs when all of the "x" particles recoil together:

$$p^*_{ba}(\pi)_{max} = \frac{\left((s-m_\pi^2 - m_x^2)^2 - 4\, m_\pi^2\, m_x^2 \right)^{1/2}}{2\sqrt{s}} \qquad (6)$$

where $s = (p_a + p_b)^2$ and $m_x^2 = (a + b)^2\, m^2$.

For $s >> m_x^2$, $p^*_{ba}(\pi)_{max} \approx \sqrt{s}\,/2$.

The radial Feynman variable (fractional momentum) is then defined as

$$x_{ab} \equiv x_{ba} = p^*_{ba}(\pi)/p^*_{ba}(\pi)_{max} \qquad (7)$$

where $p^*_{ab}(\pi)$ is the magnitude of the observed 3-momentum of the π transformed to the ab CM. Clearly $0 \leq x_{ab} \leq 1$. Along the beam direction ($\theta_{lab} = 0°$), x_{ab} is identical to the longitudinal Feynman variable

$x_F = p^*_{\parallel}/p^*_{\parallel\,(max)}$ while in the opposite direction ($\theta_{lab} = 180°$) $x_{ab} = -x_F$.

In the relativistic version of eq. (5), light cone variables $(x,\tilde{p}_\perp)$ are used in Ref. (9) instead of (p_x,p_y,p_z). The pseudo probabilities $G_A(\tilde{p})$ are then replaced by structure functions $G_{p/A}(x,\tilde{p}_\perp)$. In the ultra-relativistic limit $x \approx p_z/p_A$ is simply the longitudinal momentum fraction of the nucleon.

As we shall see, one of the most crucial aspects of SB's theory is the model shown in Fig. IIa which they proposed to evaluate $G_A(\tilde{p})$. The motivation behind their approximation is that a pion with $x_{ab} \approx 1$ could only arise from a "hard" NN collision with one of the A nucleons that carried a very large fraction of the nuclear momentum. For large enough momenta, the remaining A-1 nucleons must recoil coherently and share an equally large and opposite momentum amongst themselves. Such high momentum transfer scatterings presumably involve the hard core NN interactions, which are thought to be mediated by vector mesons (wiggly lines in Fig. II). The simplest diagram representing this completely coherent process is then the one in Fig. IIa. While at $x = 1$ (or for elastic scattering) all nucleons must recoil coherently, for smaller x, there may be considerably less coherence as we shall see.

With the above model, it is clear that G_A must be a strongly decreasing function of A since the scattering of all A nucleons as in Fig. IIa becomes more and more improbable with increasing A. Indeed, in the SB model with vector meson exchange and monopole form factors, the asymptotic form of G_A is[9]

$$G_A(\tilde{p}) = G_{p/A}(x,\tilde{p}_\perp) \sim (1 - x)^{6A-7}. \qquad (8)$$

With this model SB were able to evaluate eqs. (4,5) by parameterizing the elementary $pp \rightarrow \pi^- x$ process as

$$R(pp \rightarrow \pi x) = R_0 \ (1 - x_{pp}) \ e^{-4x_{pp}} \ e^{-15k_\perp^2} \qquad (9)$$

where x_{pp} is the pion radial Feynman variable in the pp CM, eqn. (7), and $k_\perp$ is the pion transverse momentum. Unfortunately, this fit to 6 GeV[16] and 12 GeV[17] data only provides a crude representation of the pp cross section in the 1-2 GeV region where heavy ion experiments were performed. The $x_{pp} \approx 1$ behavior may be correct, but at present the data are too scarce to be sure. This difference results in part from the prominence of the Δ_{33} resonance at these low energies[19]. We see this in Fig. III where the 6 GeV[16,18] and the more relevant 3 GeV[19] data are compared to eq. (9) and our own fits to the 3 GeV $\pi^\pm$ data:

$$R(pp \rightarrow \pi^- x, \ 3 \text{ GeV}) = R_o \ (1-x_{pp}) \ \frac{1 + x_{pp}}{1+\exp((x_{pp}-\alpha)/\beta)} \qquad (10)$$

with $\alpha = 0.45, \ \beta = 0.075,$ and

$$R(pp \rightarrow \pi^+ x, \ 3 \text{ GeV}) = R_0' \ (1-x_{pp}) \ (x_{pp}+\gamma)^{-1} \ \frac{\Gamma}{(x_{pp}-x_o)^2 + \Gamma^2/4}, \qquad (11)$$

where $\gamma = 0.3, \ x_o = 0.41, \ \Gamma = 0.22.$

We note that plotting the invariant cross section vs. x, as in Fig. III, helps hide much of the resonance structure of $d\sigma/d\Omega dk$ which is clearly seen in the data when plotted against the pion center of mass kinetic energy T_π^* (see the insert in Fig. III).

Thus, simple scaling for pp reactions as in eqn. (9) does not apply at such energies. (It has been noted[16] that π production does not even scale between 6 and 12 GeV.)

While scaling of $pp \to \pi + x$ at these energies does not hold, to develope counting rules it is still convenient to parameterize the asymptotic $x_{pp} \to 1$ behavior of the $pp \to \pi X$ cross sections as

$$R(pp \to \pi x) \underset{x_{pp}\to 1}{\sim} (1 - x_{pp})^H. \tag{12}$$

Note that $H = 1$ for all fits in eqs. (9-11).
In this way, the asymptotic form of the rates for pion production in nuclear collisions can still be simply estimated as in Ref. (9).

As a first example, SB computed $R(p + A \to \pi^-(0°) + X)$ and obtained:

$$R(p + A \to \pi^-(0°) + X) \approx R_1 (1-x_{pA})^3. \tag{13}$$

Miraculously, eqn. (13) was found[9] to be in almost perfect agreement with data[1] on π^- production in the projectile fragmentation region ($\theta^{\pi}_{lab} = 2.5°$) at all energies between 1 and 5 GeV. For $x_{pA} \lesssim 0.4$, we consider that agreement to be somewhat fortuitous because (1) eqn. (9) does not reproduce the measured $pp \to \pi^- x$ spectrum shape at these energies for $x_{pp} \lesssim 0.7$ (see Fig. III), (2) the measured pp rates do not scale (i.e., they are energy-dependent), (3) the $R(pn \to \pi^- x)$, rate which are also needed for p + A reactions, differs for $x_{pp} \lesssim 0.6$ even more from the input eqn. (9) (it is expected to be more like eqn. (11)), and (4) nuclear charge exchange π^- production ($p + A \to \pi^\circ + X' \to \pi^- + X$) is expected to be comparable in magnitude to direct $pn \to \pi^-$ for small x_{pp}, but such two step processes are neglected in eqn. (4).

Nevertheless, given the empirical fact that eqn. (13), $R \sim (1-x_{pA})^3$, provides an excellent fit to $p + A \to \pi^- (0°) + X$ data for essentially all x_{pA}, it can be used to predict $B + A \to \pi^- (0°) + X$ rates for nuclear projectiles B. Equation (5) then becomes

$$R(B + A \to \pi^-(0°) + X) = \int \frac{d^3p''}{\varepsilon(p'')} G_B(p'') R(p + A \to \pi^- + X) \mathcal{P} \quad (14)$$

where for R, eqn. (13) is to be used. Inserting eqn. (8) into eqn. (14), SB then find

$$R(B + A \to \pi^- (0°) + X) \sim (1 - x_{BA})^{6B-3}, \quad (15)$$

where this high power arises from all B-1 nucleons recoiling coherently.[9,15] Since the R input via eqn. (13) is empirically very good, eqn. (15) is on a much sounder theoretical footing than is the derivation of eqn. (13) using eqn. (9). In fact eqn. (15) reproduces[9] very well the data for $d + C \to \pi\ (2.5°) + X$ and $\alpha + C \to \pi\ (2.5°) + X$.

Observe that in the projectile fragmentation region, the power in eqn. (15) does not depend on the target A. The effect of any target with $A \geq 2$ is essentially to increase the power in eqn. (12) from H = 1 appropriate for nucleon-nucleon collisions to H = 3 in eqn. (13) due to the internal Fermi motion.[9] Note also that $x_{BA} = 1$ corresponds to a larger pion momentum than $x_{pp} = 1$, so for heavier projectiles the model is expected to work for smaller and smaller x_{BA}.

In the target fragmentation region ($\theta^{\pi}_{lab} \approx 180°$), we merely interchange $B \leftrightarrow A$:

$$R(B + A \to \pi^- (180°) + X) = R(A + B \to \pi^- (0°) + X)$$
$$\sim (1 - x_{AB})^{6A-3} = (1 - x_{BA})^{6A-3}. \quad (16)$$

Equation (16) holds only when eqn. (13) holds, i.e. for $B \geq 2$. For $B = 1$ we should use the elementary $pp \to \pi^- x$ rates; as long as eqn. (12) holds with $H = 1$ the SB prediction is[9]

$$R(p + A \to \pi^- (180°) + X) \sim (1 - x_{pA})^{6A-5}, \qquad (17)$$

which is just two powers less than eqn. (16). Since A in eqns. (16,17) tends to be much larger than the B's in eqn. (15) for the available data, backward π production represents a much more stringent test of the SB model than does forward π production. In the next section we therefore extend the work of SB by comparing eqn. (17) to data.

IV. 180° π^- PRODUCTION AND THE CLUSTER MODEL

In the target fragmentation region, eqn. (17) predicts huge powers, e.g., 6A-5 = 67 for C, and 379 for Cu, and 1243 for Pb. Furthermore, these powers are predicted to be energy independent (the variation of H in eqn. (12) with incident energy could change these numbers by at most a few units).

In Fig. IV data[20] on $p + Cu \to \pi^- (180°) + X$ are displayed. The 730 MeV data are those of Cochrane et al.[21] as analyzed by Landau,[10] and those at 5.14 and 7.51 GeV are from Baldin et al.[11] It is clear that the power fall-off is much smaller than the predicted 379. Furthermore, there appears to be a strong energy dependence of this power fall off, which the preliminary analysis of data[6] at 1 and 2 GeV also confirms.

In addition, there is evidence at both high[11] and low[10] proton energies that at any one energy the power law is fairly independent of the target. For example, at 730 MeV, $R \approx (1-x_{pA})^{13}$ for C, Cu, and Pb. If confirmed, these three pieces of experimental evidence would completely rule out eqn. (17). It must, however, also be noted that x_{pA} is not close to 1 for these data. It is possible that very close to $x_{pA} = 1$, eqn. (17) may be valid, but for the range of x_{pA} measured so far eqn. (17) does not apply.

The fact that the magnitude of the power in eqn. (17) is too large can be traced to the model of $G_A(p)$, eqn. (8), and not to uncertainties in H (in eqn. (12)) for $pp \to \pi^- x$. It was noted that eqn. (8) arose from assuming, as in Fig. IIa, that all A nucleons undergo a high momentum transfer collision to transfer all their momenta to one nucleon. Because, we consider mainly small x_{pA} in Fig. IV, it

seems very unlikely that pions produced in this region require the coherent interaction of all A nucleons. We are therefore led to consider a modification of the SB approximation for $G_A(p)$ by allowing only a subset (cluster) $c < A$ of the nucleons to have hard collisions and scatter coherently with the incoming proton. This frozen cluster model for $G_A(p)$ is specified by

$$G_A(p) \approx G_c(p) \sim (1-x)^{6c-7} \tag{18}$$

where $x = (\varepsilon(p) + p_z)\,(E(c) + p_z(c))^{-1}$ is now the longitudunal momentum fraction of the nucleon emerging from a cluster of c nucleons within the nucleus A moving with a longitudinal momentum $p_z(c)$.

In this approximation the rest of the A-c nucleons act as spectators, as illustrated in Fig. IIb. This modification of eqn. (8) is in the same spirit as the "cumulative meson production" of Baldin et al.,[11] except that we will treat carefully the Lorentz transformation in going from the pA to the pc center of mass.

The essential idea behind eqn. (18) is that it is far more probable for the incoming proton to interact strongly with a small cluster of nucleons than with the entire nucleus. Of course, giving these clusters some Fermi motion will modify the results, as we show below, but the physical picture remains the same.

With eqn. (18), eqns. (16, 17) become for $c < A$

$$R(B + A(c) \to \pi\ (180°) + X) \approx (1 - x_{Bc})^{S_{Bc}}, \tag{19}$$

$$S_{Bc} = 6c-3-2\delta_{B,1}. \tag{20}$$

On the other hand, in the projectile B fragmentation region the frozen cluster c < B model gives

$$R(B(c) + A \to \pi^- (0°) + X) \approx (1 - x_{cA})^{S_{Ac}}. \tag{21}$$

where S_{Ac} is given by eqn. (20) with $A \leftrightarrow B$.

To relate eqns. (19, 21) to data that are plotted as a function of x_{AB}, we need to transform from the BA center-of-mass frame to the Bc center-of-mass frame. This Lorentz transformation relating x_{AB} to x_{Bc} is given in the Appendix for convenience. As a function of x_{Bc}, $x_{AB}(x_{Bc})$ varies over a range 0 to $\hat{x}[B,A(c)] \leq 1$, where

$$\hat{x}[B,A(c)] \equiv x_{BA}(x_{Bc} = 1) \tag{22}$$

is the maximum momentum fraction in the BA frame that a pion carries away when the projectile B hits a small cluster of c nucleons in the target A and produces a π with $x_{Bc} = 1$ in the Bc subsystem. Therefore, as a function of x_{BA}, eqn. (19) becomes

$$R(B + A(c) \to \pi^-(180°) + X) \sim (1 - x_{Bc}(x_{BA}))^{S_{Bc}}\, \theta(\hat{x}[B,A(c)] - x_{BA}). \tag{23}$$

For pion production in the projectile fragmentation region, eqn. (21) can be expressed as a function of x_{AB} as

$$R[B(c) + A \to \pi\ (0°) + X] \sim (1 - x_{cA}\ (x_{BA}))^{S_{Ac}}\ \theta(\hat{x}[B(c),A] - x_{AB}) \tag{24}$$

where

$$\hat{x}[B(c),A] = x_{BA}(x_{cA} = 1), \tag{25}$$

and the θ function imposes the constraint that $x_{cA} < 1$ in the cluster-A center of mass.

Note that $\hat{x}[B(c),A] \neq \hat{x}[B,A(c)]$ in eqns. (22, 25) in general, i.e. the maximum x_{AB} differs for $\theta_{lab} = 0°$ and 180°. The dependence of $\hat{x}[B(c),A]$ and $\hat{x}[B,A(c)]$ on the incident energy is shown in Fig. V for two cases of interest, $p + C \to \pi^- (0°) + X$ and $p + Cu \to \pi^- (180°) + X$. The vertical bars indicate the x_{pA} range covered by the available experiments. The significance of Fig. V will be discussed below.

The effect of the θ functions in eqns. (23, 24) is to increase the effective power of the fall-off of R as a function of x_{AB}. Defining an effective slope via

$$S_{eff}(x) = \left| \frac{d \ \ell n \ R}{dx} \right|, \tag{26}$$

then as $x_{BA} \to \hat{x}[B,A(c)]$ (i.e., $x_{Bc} \to 1$)

$$S_{eff}(B + A(c) \to \pi \ (180°) + X) \approx S_{Bc}/(\hat{x}[B,A(c)] - x_{BA}). \tag{27}$$

Since $S_{Bc} << S_{BA}$ for $c << A$, and $\hat{x} \lesssim 0.4$, it is clear that S_{eff} will be much smaller in general than the predicted slope S_{BA} in the SB model.[9] Also significant is that S_{eff} now has an explicit energy dependence due to that of $\hat{x}[B,A(c)]$, as in Fig. V. Therefore, the frozen cluster model, qualitatively at least, has the behavior observed in Fig. IV.

Equations (23,24) show explicitly that a given cluster c contributes to R only in a restricted range $0 \leq x_{AB} \leq \hat{x}[B,A(c)] < 1$. This range decreases for larger cluster sizes c; for $c' < c$, we expect $p^*_{Bc'} < p^*_{Bc}$ and $\hat{x}[B,A(c')] < \hat{x}[B,A(c)]$. If we consider a pion with a fixed x_{AB},

the minimum size c_{min} of a cluster that can produce a pion with that momentum is determined by $\hat{x}[B,A(c_{min})] = x_{AB}$. The fact that different clusters may contribute to different parts of phase space has also been pointed out in Refs. (11) (where the degree of cumulativity is c_{min}). It is clear from Fig. V, that much of the 180° data shown in Fig. IV lies in the kinematic range of small clusters. We therefore show in Fig. VI (dashed curves) the fit to the $p + Cu \to \pi^-$ (180°) + X data with c = 1 and 2.

While the slopes are much closer to the slopes of the data than is the predicted S(pCu) = 379 of the SB model in eqn. (17), the data extend to x values larger than this frozen cluster model permits. Similar results were obtained with α clusters (c = 4). In fact, we find that no combination of frozen clusters can account quantitatively for the data.

We therefore conclude that for these values of x_{BA} the model of Fermi motion in both eqn. (8) and eqn. (18), illustrated in Figs. IIa,b, is inadequate. What Fig. VI shows is that additional Fermi motion, not included in eqns. (8,18), is needed to explain the range and slope of the data. In the next section we introduce a phenomenological distribution $\rho(\tilde{p})$ to account for that additional Fermi motion.

V. PHENOMENOLOGICAL FERMI DISTRIBUTION

A natural way to provide additional Fermi motion in the cluster model is to give the clusters themselves Fermi motion. Physically, such a Fermi motion arises from the interaction of a cluster with the remaining spectator nucleons as illustrated in Fig. IIc. We thus define a phenomenological pseudo-probability distributions $\rho_c(\tilde{p})$ that characterize the momentum distribution of clusters. The $\rho_c(\tilde{p})$ are phenomenological since no attempt is made here to calculate them from diagrams as in Fig. IIc, and they are pseudo-probabilities for the same reasons as $G_A(p)$ are pseudo-probabilities, i.e. because of the neglect of final state interactions in hard scattering models as used here.

The internal momentum of the cluster must then be folded into eqns. (23, 24). However, an unnecessary complication is introduced if a full three dimensional folding is performed. That is the $k_\perp$ dependence[9] of the pion production rates. In this paper we have concentrated on the longitudinal momentum dependence of those rates by focusing on $\theta^{\pi}_{1ab} \approx 0°$ and 180°. No attempt has been made to discuss finite $k_\perp$ pion production. However, if a full three dimensional folding of cluster motion is carried out, the $k_\perp$ dependence of the rates in eqns. (9, 23, 24), as well as the x_{AB} dependence would be needed.

Since ρ_c is a phenomenological distribution and the most important effect of folding for 0° and 180° production is motion along the beam axis, we avoid the uncertainties of the $p_\perp$ dependence by restricting the folding to one dimension along the beam axis. Therefore, the rates including internal cluster motion are computed via

$$R(B + A(c) \to \pi^- (180°) + X) \approx \int_{-\infty}^{\infty} dp_z \, \rho_c(p_z) \, [1-x_{Bc}(x_{BA})]^{S_{Bc}} \tag{28}$$

$$\times \{\theta(1-\hat{x}[B,A(c)]) \, \theta(\hat{x}[B,A(c)] - x_{BA})\}$$

$$= \int_{p_{max}}^{p_{min}} dp_z \, \rho_c(p_z) \, [1-x_{Bc}(x_{BA})]^{S_{Bc}}. \tag{29}$$

The extra constraint introduced into eqn. (28), $\theta(1-\hat{x}[B,A(c)])$, insures that the absolute kinematic bound on the pion momentum in the BA CM, p^*_{max}, is not exceeded; this determines p_{max}. The other constraint, $\theta(\hat{x}-x_{BA})$, requires $x_{Bc}<1$ and determines the minimum Fermi momentum, p_{min}, which can lead to a pion with the x_{BA} of interest. A similar one dimensional folding of eqn. (24) will yield the pion production rate for $\theta_{lab} \approx 0°$. We note that for large x_{AB}, p_{min} and p_{max} are generally negative. We will consider the relation of p_{min} in eqn. (29) to the k_{min} of Refs. (7,8) and to the concept of quasi-two-body scaling in Section VI.

The Fermi motion included in eqn. (28) is "minimal" or kinematic Fermi motion since we do <u>not</u> average over the energy dependence of the elementary NN cross sections. We are only folding over the p_z dependences of the x_{Bc} variables which arises from the dependence of the Lorentz transformation to the Bc CM from the BA CM and the dependence of $p^*_{Bc}(\pi)_{max}$ in eqns. (6,7).

We consider here two possible forms $\rho_c(p_z)$ that appear in the literature, both of which are independent of c. The first is a Gaussian form as observed in projectile fragmentation experiments of Greiner et al.,[22] i.e.,

$$\rho_c(p_z) \propto \exp[-p_z^2/2\ \sigma_z^2] \tag{30}$$

where $\sigma_z \approx 130$ MeV/c for all light clusters $c \geq 2$. For protons ($c = 1$), the width as determined in Ref. (22) and as estimated from a harmonic oscillator shell model is smaller, $\sigma_z \approx$ 70-90 MeV/c. However, we will use $\sigma_z = 130$ MeV/c for all clusters $c \geq 1$. As we shall see the data seem to require even a larger value of σ_z. The second form is an exponential suggested in Refs. (7,8),

$$\rho_c(p_z) \propto \exp[-|p_z|/k_o] \tag{31}$$

where $k_o \approx 100$ MeV/c.[7] (This k_o is somewhat larger than the $k_o \approx 70$ MeV/c value used most recently by Ref. (23)).

The results of the Gaussian folding for a single nucleon cluster ($c = 1$) are shown in Fig. IVa and those of the exponential folding are shown in Fig. IVb. In Fig. VI we show for comparison the results with no Fermi motion. Note again that normalizations in eqn. (28) are not determined, and we are interested here only in shapes of R. The remarkable result seen in Fig. IV is that this type of simple folding of the $pp \to \pi^- x$ rate (eqn. (10)) accounts well for both the magnitude and energy dependence of the slopes of the data. The Gaussian form leads to slightly steeper slopes, while the exponential form (with $k_o \approx 100$ MeV/c) leads to slightly flatter slopes. Overall, the exponential form seems to give the best fit.

To investigate the sensitivity of R to the cluster aspect of the model in eqn. (28), we show in Fig. VII the results for deuteron and alpha clusters ($c = 2$ and 4). While the deuteron cluster model with exponential Fermi motion (and k_o still = 100 MeV/c) fits the data as well as single nucleon clusters in Fig. IV, the α clusters do not fit as well for low energies. Possibly larger values for k_o and σ_z, or a different shape are needed. Alternately, the SB model for the (unmeasured) $p\alpha$ cross

section, $\sigma \sim (1-x)^{19}$ is inaccurate. Neverthless, it is remarkable that for high energies the results seem to be insensitive to whether clusters with c = 1, 2 or 4 are involved. For energies $E \lesssim 2$ GeV/nucleon, only c = 1 and 2 reproduce the data in our model. We note that preliminary analysis of 1.05 and 2.1 GeV proton data[6] indicates agreement with the predicted shapes in Fig. IVb for those energies. It is amusing to note that for $E \approx 300$ GeV our model gives accidentally the same slope ~ 400 as SB.

Having accounted for the $p + Cu \rightarrow \pi^-(180°) + X$ data, we turn now to $p + d \rightarrow \pi^- (180°) + X$ data of Baldin, et al.[1] and Cochran et al.[12,10] These data are particularly interesting in that they indicate (see Fig. VIII) apparent scaling for $0.7 < T_p < 8$ GeV/nucleon in sharp constrast to the $p + Cu \rightarrow \pi^- (180°) + X$ data. In fact, for this one reaction in the target fragmentation region, the SB model provides a good fit in constrast to the data in Fig. IV. The reason for this is simply that the target d only has two nucleons so that Fig. IIa can be expected to be more reliable than for Cu where 63 nucleons are required to interact coherently.

As seen in Fig. VIII, the predicted curves from eqn. (28) with c = 1 also reproduce the trend of the data. It is important to realize that within this model the energy dependence of the shape of R comes about purely from the Lorentz transformations involved in computing $\hat{x}[p,d(p)]$. We refer to the scaling displayed in $p + d \rightarrow \pi^- (180°) + X$ as only "apparent" since it results from the weak energy dependence of $\hat{x}[p,d(p)]$, in constrast to the stronger energy dependence of $\hat{x}[p,Cu(p)]$ in Fig. V. Therefore, apparent scaling in this reaction is a kinematical effect. We shall see below that the apparent scaling of $B + A \rightarrow \pi^- (0°) + x$ is also kinematical in origin.

Before turning to the projectile fragmentation data, we note that preliminary analysis of the data[6] on $\alpha + Cu \rightarrow \pi^-$ (180°) + X at 1.05 and 2.1 GeV/nucleon also agrees with the shapes predicted from eqn. (28) and shown in Fig. IX.

We therefore find that all available data on backward π production can be accounted for by eqn. (28) with c = 1, or 2 and the exponential form for $\rho(p_z)$ in eqn.(31).

A critical second test of the above model is pion production in the projectile fragmentation region, where the SB model is known to work well. We therefore want to find out if eqn. (28) also reproduces those data and if so, why the SB model works in this region but not in the backward π region.

In Fig. X, the data at Papp et al.[1] on $p + C \rightarrow \pi^-$ (2.5°) + X is shown together with the results of eqn. (28) (A and B now being interchanged in this projectile fragmentation region). Note that the $x_{pC} \gtrsim 0.6$ shapes are indeed reproduced, but for smaller x_{pC} substantial deviations are found (note too the large deviation between fit SB and fit A for $x_{pC} \lesssim 0.4$). In the small x_{pC} region, rescattering, pion absorbtion, and charge exchange, not included in a hard scattering model like eqn. (28), can be expected to decrease the results greatly.[24] As expected, the main deviations in fact occur for the region of x_{pC}'s where the Δ_{33} dominates (see Fig. III inserts) and the pions have the highest scattering and absorbtion cross sections. The deviation and Δ_{33} dominance is even more apparent for π^+ (Fig. XI) where $d^2\sigma/d\Omega dk[pC \rightarrow \pi^+ X]$ data actually show a peak, at the resonance energy.

The remarkable point to note in connection with Figs. X,XI is again the apparent scaling that follows from eqn. (28) in the projectile fragmentation region in agreement with data. That this apparent scaling is again only a kinematical effect can be seen in Fig. V which shows that $\hat{x}[p,C(p)]$ in the projectile fragmentation region is a very weak function of energy, and that $\hat{x}[p,C(c \geq 1)]$ is very close to 1. The additional folding in eqn. (28) simply extends the range of the cluster contribution a little closer to 1. This is in sharp constrast to the target fragmentation region where $\hat{x}[p,Cu(p)]$ (see Fig. V) is small thereby making the influence of the folding in eqn. (28) much larger. Consequently, the shapes of the rates R in the projectile fragmentation region are rather insensitive to the specific dynamical model of $G_A(p)$ or $\rho(p)$. In fact all three models in Fig. II give essentially the same agreement with data in the high x_{pC} region in Fig. X.

Turning to the $dC \to \pi^-$ (2.5°)X and $\alpha C \to \pi^-$ (2.5)X data in Figs. XII, we again find that our model leads to apparent scaling as seen in the data. For these reactions the shapes of the data are somewhat better reproduced with the Gaussian folding than with the exponential folding. However, we emphasize that we have made no attempt to find the single best function $\rho(\tilde{p})$ to account for all reactions in the projectile and target fragmentation region. Our philosophy has been simply to take $\rho(\tilde{p})$ from other sources in eqs. (30,31) as the input to eqn. (28). Since most data fall between the Gaussian and exponential fits, we expect that there is an optimal choice for $\rho(\tilde{p})$ bounded by eqns. (30,31).

VI. RELATION TO QUASI-TWO BODY SCALING[8] (QTBS)

In this section we compare our model, eqn. (28), with the hard scattering models of Amado and Woloshyn[7] and Frankel et al.[8,23] that have led to the concept of QTBS. The main differences are (i) the choice of the kinematic constraint $\mathcal{P}$ in eqns. (4,5) and p_{min}, p_{max} in eqn.(28), (ii) the parameterization of the elementary $pp \to \pi X$ rate, and (iii) the way the integration in eqn. (28) is approximated.

The kinematic constrain in Refs. (7,8) follows from assuming that final state interactions can be neglected, as in Fig. Ib, and that the exchanged (virtual) cluster p' is not part of the energy constraint.

For pion production, the minimum cluster momentum $\tilde{p}_c = \tilde{p}' \equiv \tilde{k}_{min}$ necessary to produce a pion of momentum $\tilde{k}_\pi$ is determined by[23]

$$\sqrt{p_B^2 + m_B^2} + m_A = \sqrt{k_\pi^2 + m_\pi^2} + \sqrt{(\tilde{p}_B - \tilde{k}_\pi + \tilde{k}_{min})^2 + m_{B+c}^2} + \sqrt{k_{min}^2 + m_{A-c}^2}\,, \qquad (32)$$

where p_B is the beam B momentum, c is the cluster size, A is the target, $m_{B+c} = (B+c)m$, and $m_{A-c} = (A-c)m$. Equation (32) expresses simply energy conservation for B "sticking" to c, but without other final state interactions.

On the other hand, if the theory were more realistic and included final state interactions, then the π,B,c, and A-c in eqn. (32) would also be virtual and the specific constraint of eqn. (32) need no longer apply. In this case it seems more consistent to build a model which simply imposes the energy constraint on the B + c collision vertex

directly and thus requires somewhat smaller values of internal nuclear momenta $\tilde{p}' = \tilde{p}_c \equiv \tilde{p}_{min}$:

$$\sqrt{p_B^2 + m_B^2} + \sqrt{p_{min}^2 + m_c^2} = \sqrt{k_\pi^2 + m_\pi^2} + \sqrt{(\tilde{p}_B - \tilde{k}_\pi + \tilde{p}_{min})^2 + m_{B+c}^2} \,. \tag{33}$$

Of course if one had a complete theory, as opposed to simple hard scattering models, then all final state interaction would be included and overall energy conservation would be insured. In the present cases, however, we believe that eqn. (33) is better-particularly when integrated with the analytic $Bc \to \pi x$ rate, as in eqn. (29), and when combined with the requirement that $\tilde{k}_\pi$ be less than the maximum momentum in that direction from the $B + A \to \pi + X$ reaction.

Both p_{min} and k_{min} are shown in Fig. XIII for different beam energies as a function of x_{pCu} and $(k_\pi)_{lab}$. Here the positive values refer to a direction opposite to the beam. Although p_{min} and k_{min} both cross zero at roughly the same pion momentum, $p_{min} < k_{min}$ for the important large pion momenta.

We now come to the second and third points, namely, the parameterization of $pp \to \pi x$ and the approximation of the integral in eqn. (28). In Ref. (23) the arguments of Refs. (7,8) for proton inclusive rates were extended to pion inclusive rates. The main assumption is that the elementary rates inside the integral are slowly varying functions of the cluster momentum and can be pulled outside the integral. Then for $k_{min} \gtrsim k_o \approx 100$ MeV/c, the integral in eqn. (28) can be approximated

as

$$R \propto \rho(k_{min}) \propto e^{-k_{min}/k_o} . \qquad (34)$$

First it is clear that eqn. (34) can be applied only for the limited range of data where $k_{min} > k_o$. As seen from Fig. XIV, that range is strongly energy dependent and is bounded below by a minimum x_{pCu} value, $x_{min} \approx 0.28$ for 730 MeV, 0.17 for 2.1 GeV, and 0.08 for 7.5 GeV data. From Fig. IV this range of applicability is seen to cover only about a half of the x_{pCu} range of the available data. In the projectile fragmentation region the range of applicability is even more limited with $x_{min} \approx 0.9$ for $p + C \rightarrow \pi + x$ at 2 GeV.

We have verified though that in the limited (energy dependent) range of its applicability, eqn. (34) does provide a reasonable fit to the shapes of these data.

There is however an important caveat in the interpretation of k_o in eqn. (34) that can be seen from eqn. (28). This concerns the momentum dependence of the elementary subprocess in eqn. (28). If we approximate R by $\exp(-|p_{min}|/k_o)$ for $|p_{min}| \gtrsim k_o$ (replacing k_{min} by p_{min}) then we find that the slopes predicted are flatter than those obtained with k_{min} and thus agree less well with the data. However, including the momentum dependence of the $pp \rightarrow \pi x$ rates leads to the slope observed in the data. We therefore conclude that this strong effect of the momentum dependence of the elementary rates must be buried phenomenologically in eqn. (34). Therefore not only final state interactions, as pointed out in Ref. (14), but also off shell effects and the momentum dependence of the elementary pion production rates cloud any simple interpretation of the exponential form in eqn. (34).

Quasi-two body scaling seems then to be a remarkable phenomenology[26] over its limited range of applicability which is however difficult to interpret theoretically.

VII. SUMMARY AND CONCLUSION

Our main result is the success with which the shapes of the inclusive pion production cross sections in both the projectile and target fragmentation regions are accounted for by the simple hard scattering model given by eqn. (28). A simplifying - but powerful - feature of this model is the invariant parametization of the $pp \to \pi x$ and $pc(\text{cluster}) \to \pi x$ rates in terms of the Feynman scaling variable "x_{pc}". In this regard we follow closely the work of Schmidt and Blankenbecler.[9] In particular, we find that the magnitude as well as the energy dependence (i.e. non-scaling) of the slopes of the nucleus-nucleus pi production cross sections are correctly obtained by simply averaging elementary $pp \to \pi x$ rates over internal nucleon momenta with an exponential pseudo-Fermi distribution in eqn. (28). The shapes of the cross sections from 700 MeV to 7.5 GeV can be so explained.

Although elementary nucleon-nucleon collisions provide one explanation, we find that projectile - light cluster collisions also provide a possible explanation of these shapes. Specifically, the data in the target fragmentation region ($\theta^{\pi}_{lab} \approx 180°$, $A_T \gg A_p$) rule out production from large clusters, such as the $c = A_T$ model of Ref. (9). However, production from 2 or 3 nucleon clusters is compatible with the data as long as these clusters are assumed to have the same Fermi motion distribution. At present we consider the dependence of the Fermi distribution on cluster size an open question. The measurements of Greiner et al.[22] tend to indicate very little c dependence, in contrast to the models considered in Refs. (12, 13) which assume increasingly broader distributions with cluster size.

After non scaling in the target fragmentation region was analyzed, we investigated why there was "apparent scaling" of pion production in the projectile fragmentation region.[1] We find that this apparent scaling is largely due to kinematic (Lorentz transformation) effects. As illustrated in Fig. V, the projectile fragmentation region is rather insensitive to the dynamical details of the production mechanism. In fact, any cluster c, including the $c = A_T$ model of Ref. (9), can explain the shape of these data at $x_{AB} \sim 1$.

Since exponential tails to Fermi distributions have been receiving much attention lately[7,8,23] and since they also appear to be important in relativistic heavy ion collisions, it is essential to understand some of the physics buried in the empirical distribution $\rho(k) \sim \exp(-k/k_o)$ that was used in eqn. (28). After analyzing Fig. Ia and b and investigating the range of momenta which may contribute in each, it became clear that $\rho(\tilde{k})$ is not proportional to $|\psi_A(\tilde{k})|^2$, the real probability of finding a nucleon of momenta $\tilde{k}$ in the nucleus. The complex final state interactions, as well as the unknown off-shell $pp \to \pi x$ amplitudes are mixed in $\rho(k)$ in a way which does not permit an obvious separation of the structure and reactive parts. We are therefore forced to regard $\rho(k)$ as a phenomenological function that appears to be universal for the range of reactions studied so far.

The primary value of the model presented here lies in its ability to gauge the relative importance of (1) simple kinematics (multiple Lorentz transformations), (2) production on multi-nucleon clusters (or correlations), and (3) Fermi motion within the nucleus. In addition, this model has the purely phenomenological value of succintly summarizing the shapes of a wealth of experimental data.

It is clear that much more theoretical work is needed to understand why such a simple form for $\rho(k)$ and the hard scattering model work so well for pion production from both nucleons and clusters. In any case, we agree with Ref. (14) that a simple, unambiguous physical interpretation of $\rho(k)$ is not as yet possible.

To calculate absolute normalizations, extensions of the present model are obviously required. In this paper we have focused only on the shapes of the cross sections in order to keep the analysis of the essential physics as simple and transparent as possible. One existing approach that does provide normalizations and does include the results of the hard scattering model in lowest order is the intra-nuclear cascade model with multiple scattering and absorption.[25] However, the price paid in such models is a large number of assumptions combined with great numerical complexity, from which the relative importance of different physical effects is often difficult to extract.

For the future, we suggest that experiments on pion production concentrate on the target fragmentation region with beams of low energy $E \lesssim 2$ GeV/nucleon (particularly < 700 MeV) and of course look for pions with as large momenta as possible. As demonstrated in Figs. IVa and b, the predictions of the theory are more sensitive to reaction dynamics and nuclear structure at the lower energies. In this regard we note that since relativistic projectiles up to ^{56}Fe are now available, the target fragmentation region could perhaps be more easily studied via the $A_P + A_T \rightarrow \pi\ (0°) + X$ reaction where $A_P(Ar,Fe) >> A_T(p,d)$.

Other experiments of considerable interest would be $p + A \rightarrow \pi(0°, 180°) + X$ with light targets, A = d,α etc., since the elementary rates, e.g. $(1-x)^{3,7}$, used in a hard scattering model such as eq. (28) have been tested only for large A. Finally, we note that the elementary $p + p \rightarrow \pi + x$ rates also need further experimental study and compilation in the energy range between 0.5 and 3 GeV.

ACKNOWLEDGEMENTS

We are most grateful to Lee Schroeder, Steve Chessin, J. Geaga and J. E. Grossiord for bringing their preliminary data[6] as well as other data[11] to our attention. Their finding of non-scaling inthe target fragmentation region was the stimulus for much of this work. We have also profited from discussions with Morton Weiss, Richard Woloshyn and Yasha Karant. Finally we wish to thank Art Pozkanzer, Dave Hendrie and members of the Nuclear Theory Group at LBL for constructive criticisms.

APPENDIX

We note here for convenience the Lorentz transformation relating x_{AB} and x_{Bc} in eqs. (22-25, 28, 29). We consider only the case when the pion momentum and the cluster c lab momentum $\tilde{p}_c$ are parallel to the beam momentum $\tilde{p}_B$. The target A is assumed to be at rest in the lab. Then for pions produced in the projectile (+), target (-) fragmentation regions

$$x_{Bc}(x_{AB}) = \frac{p^*_{AB}(\pi)}{p^*_{Bc}(\pi)} \gamma_{ABc} \left\{ x_{AB} \pm \beta_{ABc} \sqrt{x^2_{AB} + m^2_\pi/(p^*_{AB}(\pi))^2} \right\}, \qquad (A.1)$$

where β_{ABc} is the relativistic velocity difference of the Bc center-of-mass minus the AB center-of-mass velocities, $\gamma_{ABc} = (1-\beta^2_{ABc})^{1/2}$, and $p^*_{AB}(\pi)$ is given by eqn. (6). The expression of $x_{AB}(x_{Bc})$ is of course given substituting $A \leftrightarrow c$ above and changing $\pm \to \mp$. The maximum momentum fraction in the BA frame is then given by eqn. (22) for the target fragmentation region

$$\hat{x}[B,A(c)] = \gamma_{ABc} \left\{ p^*_{Bc}(\pi) + \beta_{ABc} \sqrt{p^{*2}_{Bc}(\pi) + m^2_\pi} \right\} / p^*_{AB}(\pi) \qquad (A.2)$$

and by eqn. (25) for the projectile fragmentation region

$$\hat{x}[B(c),A] = \gamma_{BAc} \left\{ p^*_{Ac}(\pi) - \beta_{BAc} \sqrt{p^{*2}_{Ac}(\pi) + m^2_\pi} \right\} / p^*_{AB}(\pi) \qquad (A.3)$$

where β_{BAc} is the velocity difference between the Ac center-of-mass and the AB center-of-mass.

REFERENCES

1. J. Papp, J. Jaros, L. Schroeder, J. Staples, H. Steiner, A. Wagner, and J. Wiss, Phys. Rev. Lett. 34, 601 (1975); J. Papp, LBL-3633, Ph. D. Thesis, unpublished (1975).

2. S. Nagamiya, I. Tanihata, S. Schnetzer, L. Anderson, W. Brückner, O. Chamberlain, G. Shapiro, and H. Steiner, LBL-6770, Proceedings of VIIth Int. Conf. on High Energy Physics and Nuclear Structure, Zürich (1977).

3. K. Nakai, J. Chiba, I. Tanihata, S. Nagamiya, H. Bownan, J. Ioannous, and J. O. Rasmussen, Proceedings of VIIth Int. Conf. on High Energy Physics and Nuclear Structure, Zürich (1977).

4. J. Gosset, H. H. Gutbrot, W. G. Meyer, A. M. Poskanzer, A. Sandoval, R. Stock, and G. D. Westfall, Phys. Rev. C16, 629 (1977).

5. M. M. Gazzaly, J. B. Carroll, J. V. Geaga, G. Igo, J. B. McClelland, M. A. Nasser, H. Spinka, A. L. Sagle, V. Perez-Mendez, R. Talaga, E. T. B. Whipple, and F. Zarbakhsh, LBL-7278 preprint (1978).

6. S. Chessin, J. Geaga, J. E. Grossiord, D. Hendrie, L. Schroeder, B. Treuhaft, K. van Bibber and E. Wuest, Bull. Am. Phys. Soc. 23, 48 (1978).

7. R. D. Amado, R. M. Woloshyn, Phys. Rev. Lett. 36,1435 (1976).

8. S. Frankel, Phys. Rev. Lett. 38, 1338 (1977);
S. Frankel, W. Frati, Phys. Rev. C16, 1499 (1977).

9. I. A. Schmidt, R. Blankenbecler, Phys. Rev. D15, 3321 (1977).

10. R. H. Landau, LBL-7169, Jan. 1978, to be published in Phys. Rev. C.

11. A. M. Balin, N. Giordenescu, V. N. Zubarev, L. K. Ivanova, N. S. Moroz, A. A. Povtoreiko, V. B. Radomanov and V. S. Stavinskii, Yad. Fiz. 20, 1201 (1974) [Sov. J. Nucl. Phys. 20, 629 (1975)]; A. M. Baldin et al. Yad. Fiz. 18, 79 (1973) [Sov. J. Nucl. Phys. 18. 41 (1974)]; Yad. Fiz. 21, 4008 (1975), [Sov. J. Nucl. Phys. 21, 5171 (1976).

12. V. V. Burov, V. K. Lukyanov, and A. I. Titov, Phys. Lett. 67B, 46 (1977) and Dubna preprint E2-10680 (1977).

13. T. Fujita, Phys. Rev. Lett. 39, 174 (1977).

14. R. D. Amado, R. M. Woloshyn, Phys. Letts. 69B, 400 (1977), Phys. Rev. C 16, 1255 (1977).

15. R. D. Amado, Phys. Rev. C14, 1264 (1976).

16. E. Gellert, LBL-784 (unpublished) 1972, "The Inclusive $pp \to \pi^-$ + Anything at 6.6 GeV/c Compared to High Energies."

17. C. W. Akerlof, et al. Phys. Rev. D3, 645 (1971).

18. M. E. Law, J. Kasman, R. S. Panvini, W. H. Sims, and T. Ludlam, LBL-80, August 1972, "A Compilation of Data on Inclusive Reactions".

19. A. C. Melissinos, G. G. Fazio, T. Yamanouchi, S. J. Lindenbaum and L. C. L. Yuan, Phys. Rev. Letts. 7, 454 (1961).

20. We are very grateful to L. Schroeder, S. Chessin, and J. Geaga for bringing Ref. 11 to our attention along with their preliminary data on $p + Cu \to \pi^-$ at 1 and 2 GeV which shows a striking energy dependence, (see Ref. 6).

21. D. R. F. Cochran, P. N. Dean, P. A. M. Gram, E. A. Knapp, E. R. Martin, D. E. Nagel, R. B. Perkins, W. J. Shlaer, H. A. Thiessen and E. D. Theriot, Phys. Rev. D6, 3085 (1972).

22. D. E. Greiner, P. J. Lindstrom, H. H. Heckman, B. Cork and F. S. Bieser, Phys. Rev. Lett. 35, 152 (1975).

23. C. F. Perdrisat, S. Frankel and W. Frati, Univ. of Penn. Preprint, UPR 052, 3/16/78, "Quasi-Two-Body Scaling in Nuclear Pion and Proton Production by Protons, Deuterons and Alpha Particles".

24. M. M. Sternheim and R. R. Silbar, Phys. Rev. D6, 3117 (1972); Phys. Rev. C8, 492 (1973); D. A. Sparrow, M. M. Sternheim and R. R. Silbar, Phys. Rev. C10, 2215 (1974).

25. A. A. Amsden, J. N. Ginocchio, F. H. Harlow, J. R. Nix, M. Danos, E. C. Halbert, R. K. Smith, Phys. Rev. Lett. 38, 1055 (1977). R. K. Smith, Proceeding of the Falls Creek Falls Meeting on Heavy Ion Collisions, June 1977. p. 363, Conf. - 770602.

26. We note an amusing, purely phenomenological, extension of eqn. (34) that seems to work miraculously on the entire range of data considered in this paper. That is to remove the absolute value on k_{min} and simply allow k_{min} to have negative values i.e., $\vec{k}_{min}$ along the beam direction as in Fig. XIII. Plotting $\exp(-k_{min}/k_o)$ with $k_{min}(x_{pCu})$ from Fig.XIII reproduces the shapes of all data as well as eqn.(28) in Fig. IV. Even the $(1-x_{pC})^3$ shape in Fig. X is reproduced in the projectile fragmentation region. We can attribute no physical significance to this numerology though.

FIGURE CAPTIONS

Fig. I. (A) General Feynman diagram for $p + A \to \pi + X$ in hard scattering models. ψ_A is the nuclear vertex function, $T_{pp'\pi x}$ the off-shell π production amplitude, and Ω is the distortion factor which includes all final state interactions. In (B) the final state interactions are neglected and $T_{pp'\pi x}$ is evaluated on-shell.

Fig. II. Three models of the pseudo-probability distribution for finding a nucleon with momentum $\tilde{p}$ within the nucleus. (A) The completely coherent model used in Ref. (9). (B) The frozen cluster model in which "c" nucleons act coherently. (C) The cluster model with Fermi motion in which the "c" coherent nucleons are given a CM motion of their own.

Fig. III. The invariant cross section for $pp \to \pi^{\pm} X$ versus the radial fractional momentum $x_R = x_{pp}$. The circles are the 2.9 GeV data of Melissios et al.[19] and the boxes are the 5.7 GeV data of Gellert.[16] The solid curves are the fits to these cross sections given by eqns. (10,11) and used as input to our model, eqn. (28). The dashed curve is the fit of Ref. (9) to 6 and 12 GeV data. The inserts, which show $d\sigma/d\Omega dk$ as a function of the CM pion kinetic energy T_π^*, reveal the Δ_{33} dominance.

Fig. IV. The invariant cross section for $pCu \to \pi^- (180°) X$ vs x_{pCu}. The 730 MeV data are from Cochran et al.,[21,10] the 5.14 and 7.50 GeV data are from Baldin et al.[11] The curves are calculated with a model employing elementary $pp \to \pi X$ collisions ($c = 1$ in eqn. (28)). In (A) a Gaussian shape is used for the pseudo-Fermi distribution, in (B) an exponential shape is used.

Fig. V. The dependence of $\hat{x}[B,A(c)]$, the pion fractional momentum x_{AB} for which $x_{Bc} = 1$, for pion production from various frozen "clusters" within the nucleus. The lower curves are for pions in the target fragmentation region; the upper curves are for the beam fragmentation region. The vertical bars show the range of x_{pA} values covered by Refs. (6,11). The target fragmentation region is clearly much more sensitive to clustering aspects.

Fig. VI. The invariant cross sections for $pCu \to \pi^-$ (180°)X calculated in a model employing elementary $pd \to \pi X$ collisions (A) or elementary $pp \to \pi X$ collisions (B). The dashed curves are for production on "frozen" clusters. The solid curves are for production on clusters with exponential Fermi motion.

Fig. VII. Invariant cross section for $pCu \to \pi^-$ (180°)X calculated in a model, eqn. (28), employing elementary $pd \to \pi X$ collisions (A) or elementary $p\alpha \to \pi X$ collisions (B). The dashed curves are for exponential Fermi motion of the clusters, the solid curves are for Gaussian distributions.

Fig. VIII. Invariant cross sections for $pd \to \pi^-$ (180°)X calculated in our model employing elementary $pp \to \pi X$ collisions. Both the calculations and the data [730 MeV - Ref. (21,10); 5.14, 7.5 GeV - Ref. (11)] show "apparent" scaling for this light target - in contrast to the previous figures.

Fig. IX. Invariant cross section for $\alpha Cu \to \pi^- (180°)X$ vs. $x_{\alpha Cu}$ for 1.05 and 2.1 GeV/N beam energies calculated in a model employing elementary $\alpha d \to \pi X$ and $\alpha p \to \pi X$ collisions. The preliminary data of Ref. (6) tend to fall within the solid and dashed curves. Normalizations are arbitrary.

Fig. X. Invariant cross section for $pC \to \pi^- (2.5)X$ calculated with elementary $pp \to \pi X$ collisions parameterized in terms of the "SB" and "A" fits of Fig. III. Only for $x_{pC} \gtrsim 0.6$ do these fits agree with $(1-x_{pC})^3$. Data are from Ref. (1).

Fig. XI. The invariant cross section[1] and the doubly differential cross section for $pC \to \pi^+ (2.5°)X$ calculated with the elementary $pp \to \pi X$ parameterization of Fit B in Fig. III. $d^2\sigma/d\Omega dk$ shows the Δ_{33} dominance more clearly than the invariant cross section.

Fig. XII. The invariant cross section for $dC \to \pi^- (2.5°)X$ and $\alpha C \to \pi^- (2.5°)X$ as calculated in the model employing elementary $pC \to \pi^- X$ and $dC \to \pi^- X$ collisions. The dot-dashed curves is calculated with no Fermi motion. The data are from Ref. (1).

Fig. XIII. Minimum Fermi momentum p_{min} and k_{min} of a nucleon inside the nucleus necessary to produce a pion in the reaction $p + Cu \to \pi^- (180°) + X$ at a given x_{pCu} and k_π^* in the pCu center-of-mass. Solid curves show p_{min} from eqn. (33); dashed curves show k_{min} of Ref. (23) from

eqn. (32). Incident kinetic energies of 0.73, 2.1, 7.5 GeV are shown. Positive values correspond to momenta opposite to the beam direction. Fermi motion dominates in the range of x_{pCu} and k_{π}^{*} for which $k_{min} \gtrsim +100$ MeV/c leading to eqn. (34).

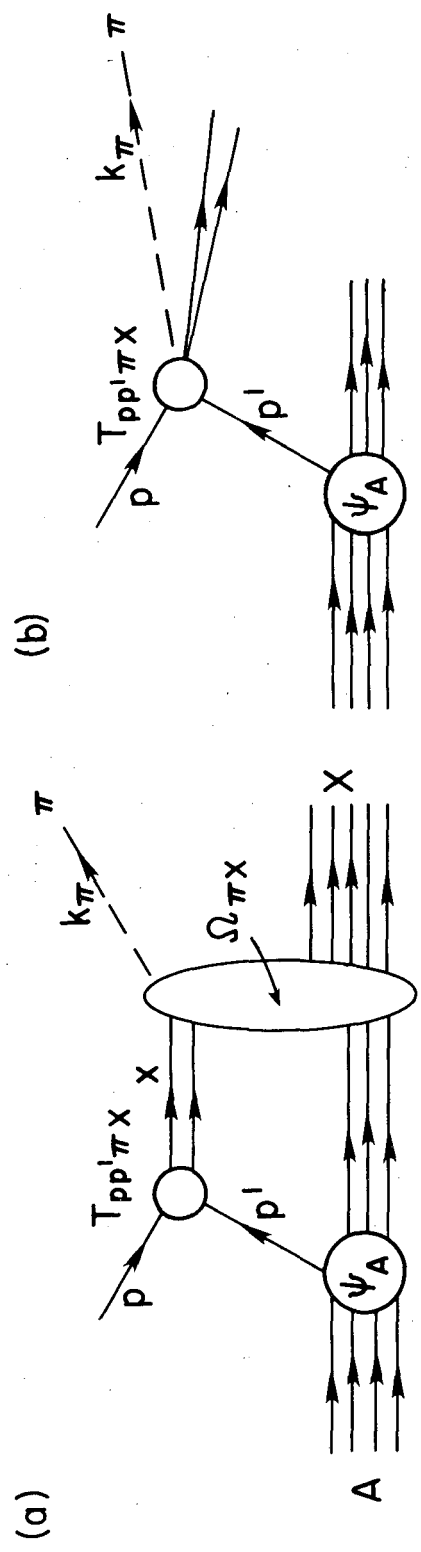

XBL784-679

Fig. I

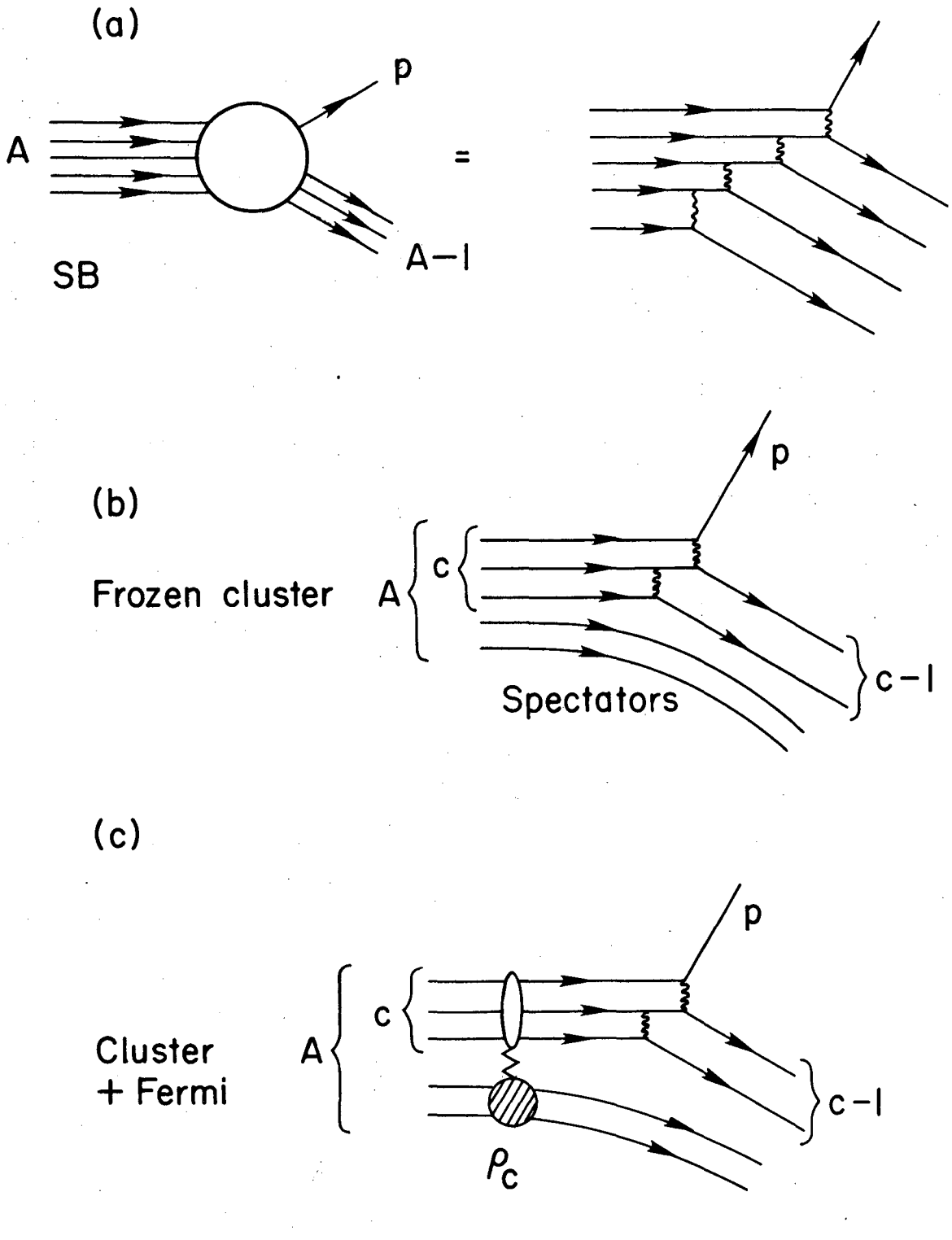

XBL784-678

Fig. II

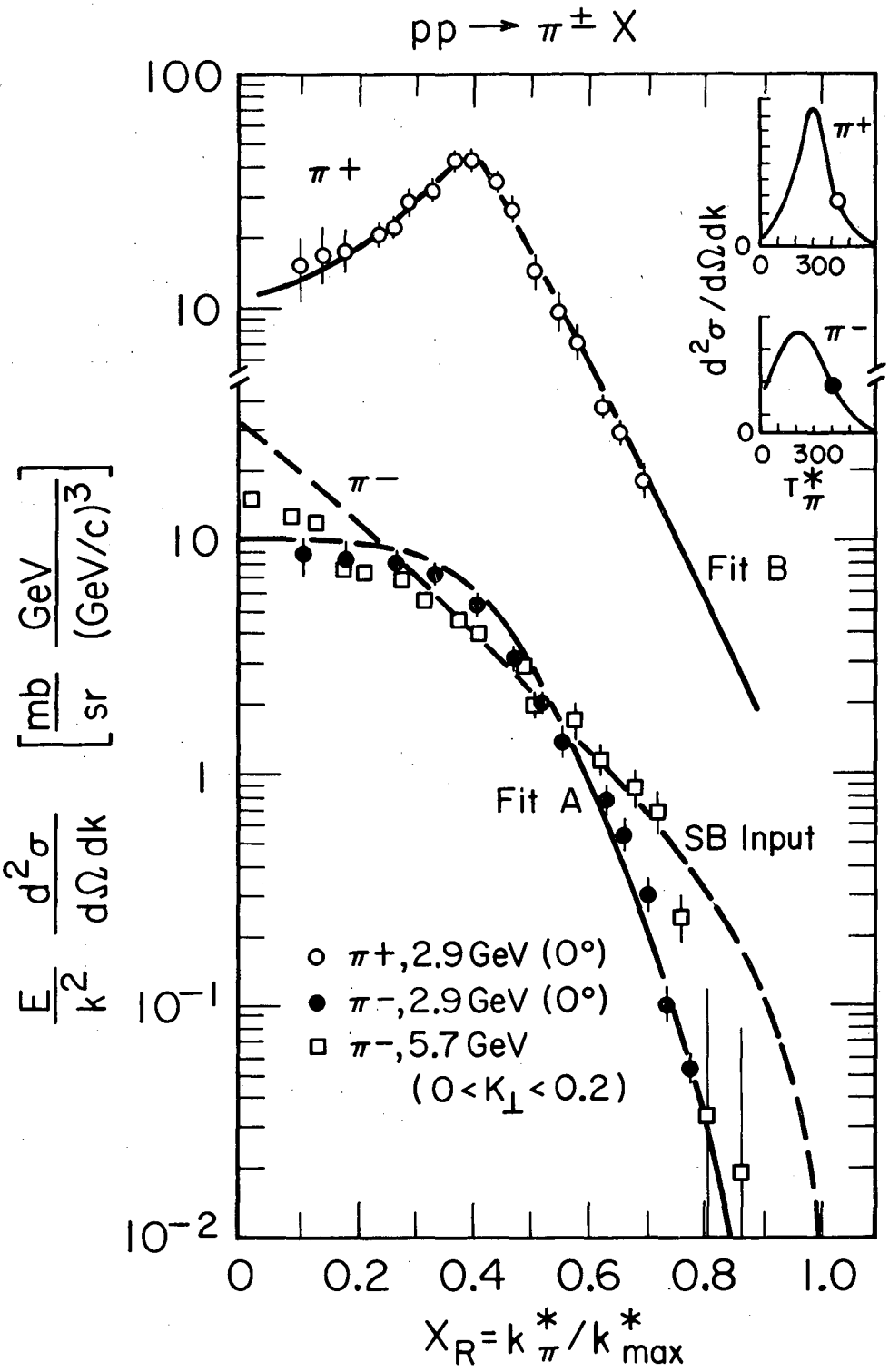

XBL 784 – 681

Fig. III

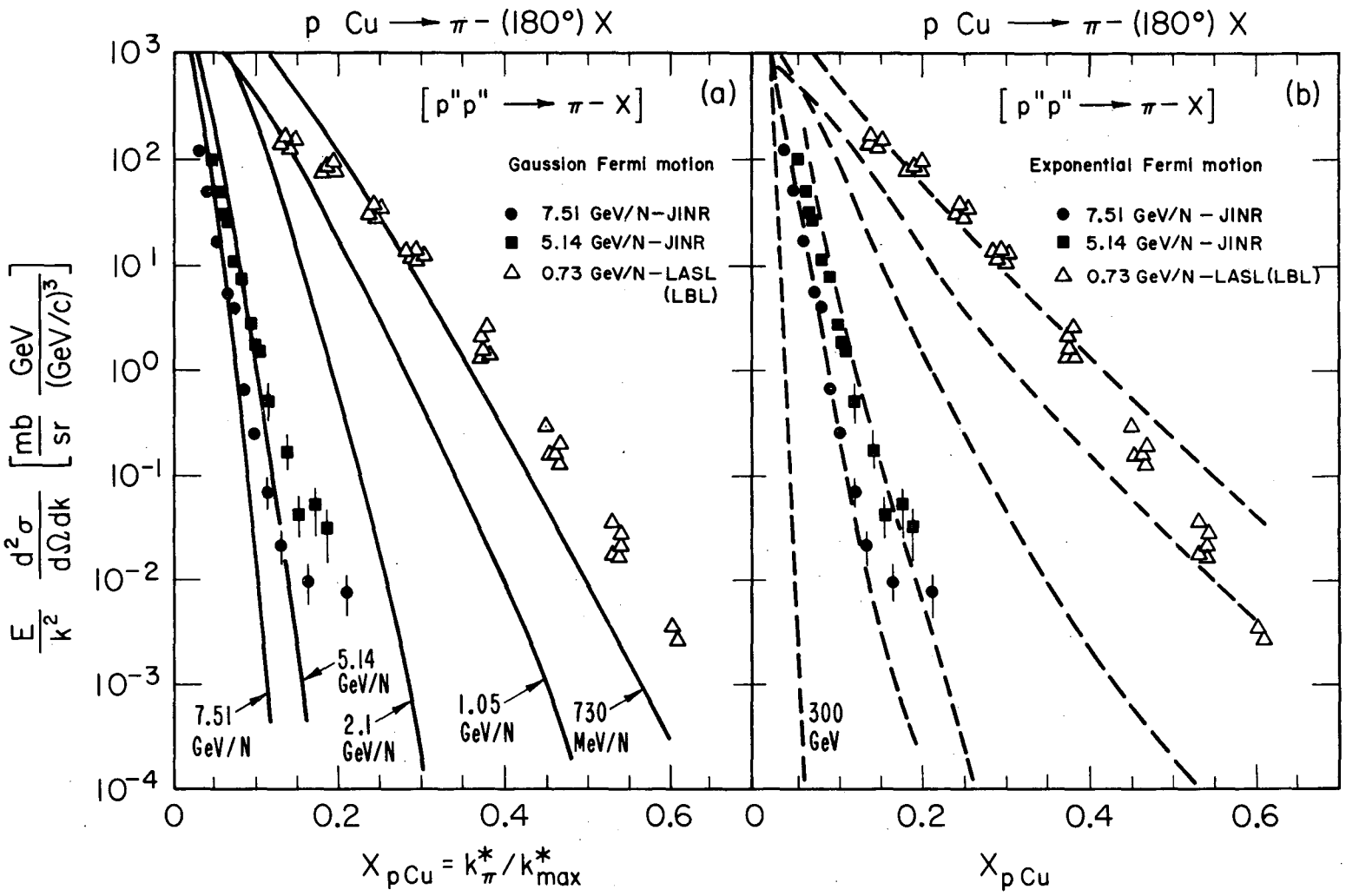

XBL 784 – 688

Fig. IV

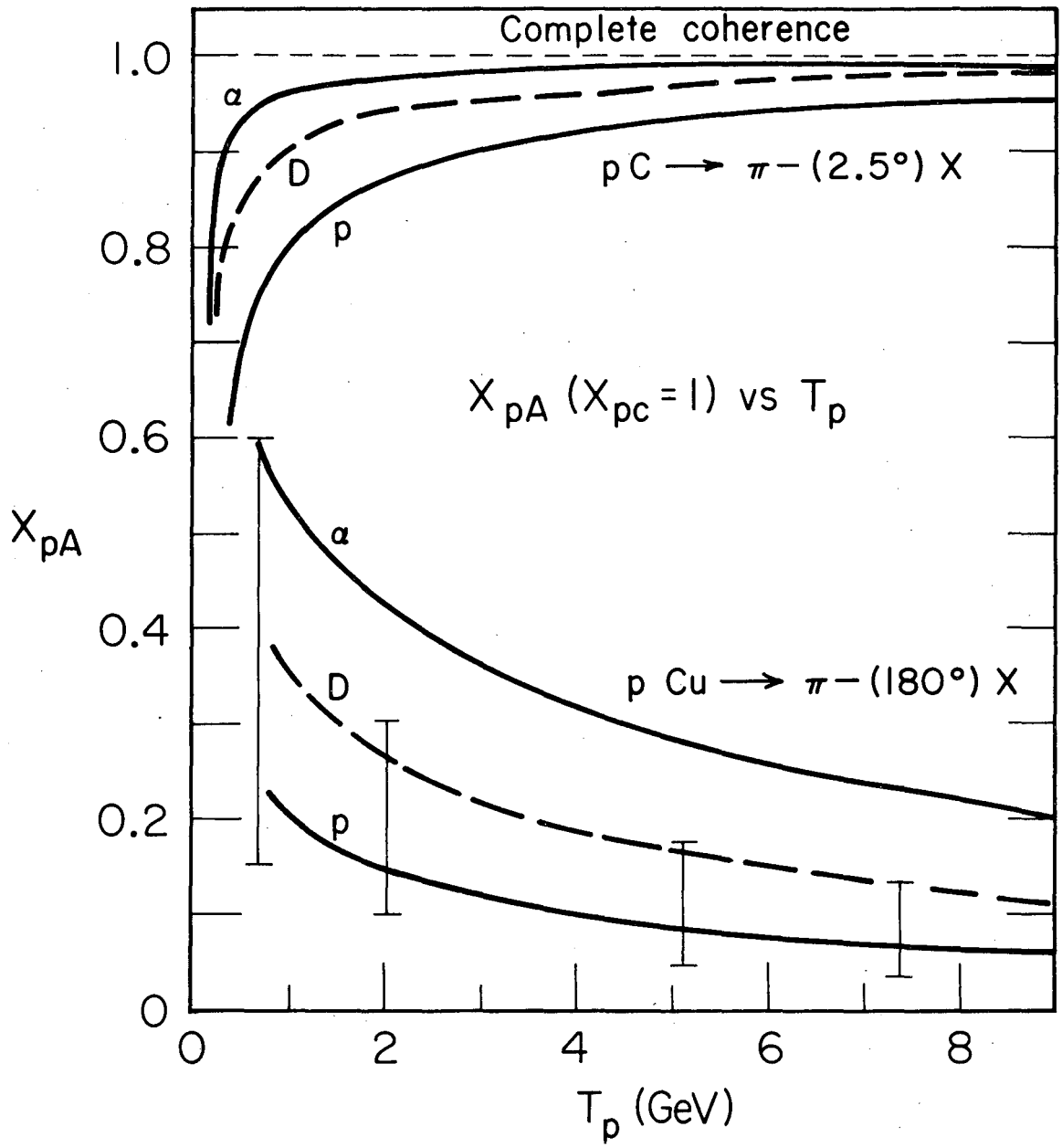

XBL 784-680

Fig. V

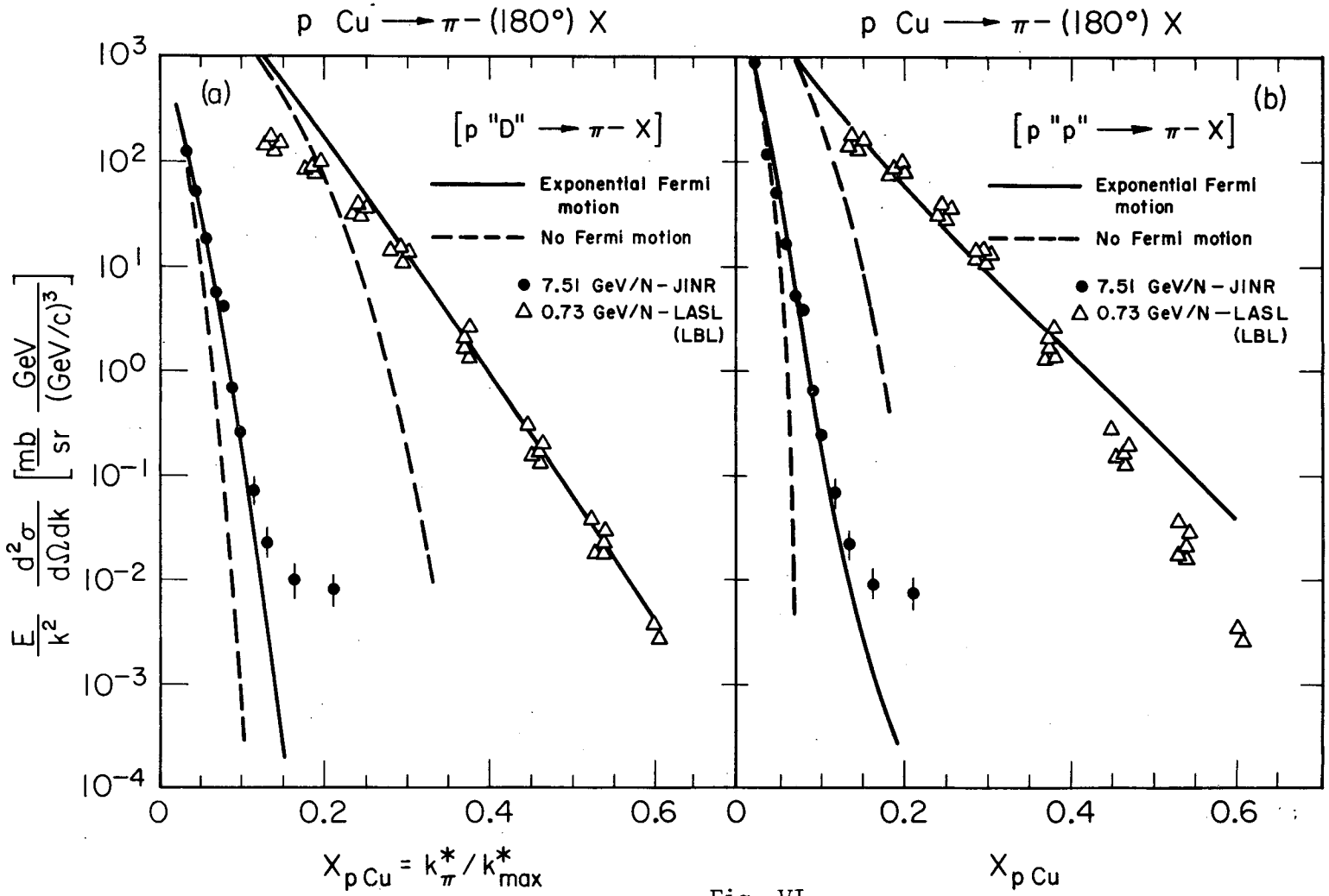

Fig. VI

XBL 784-8257

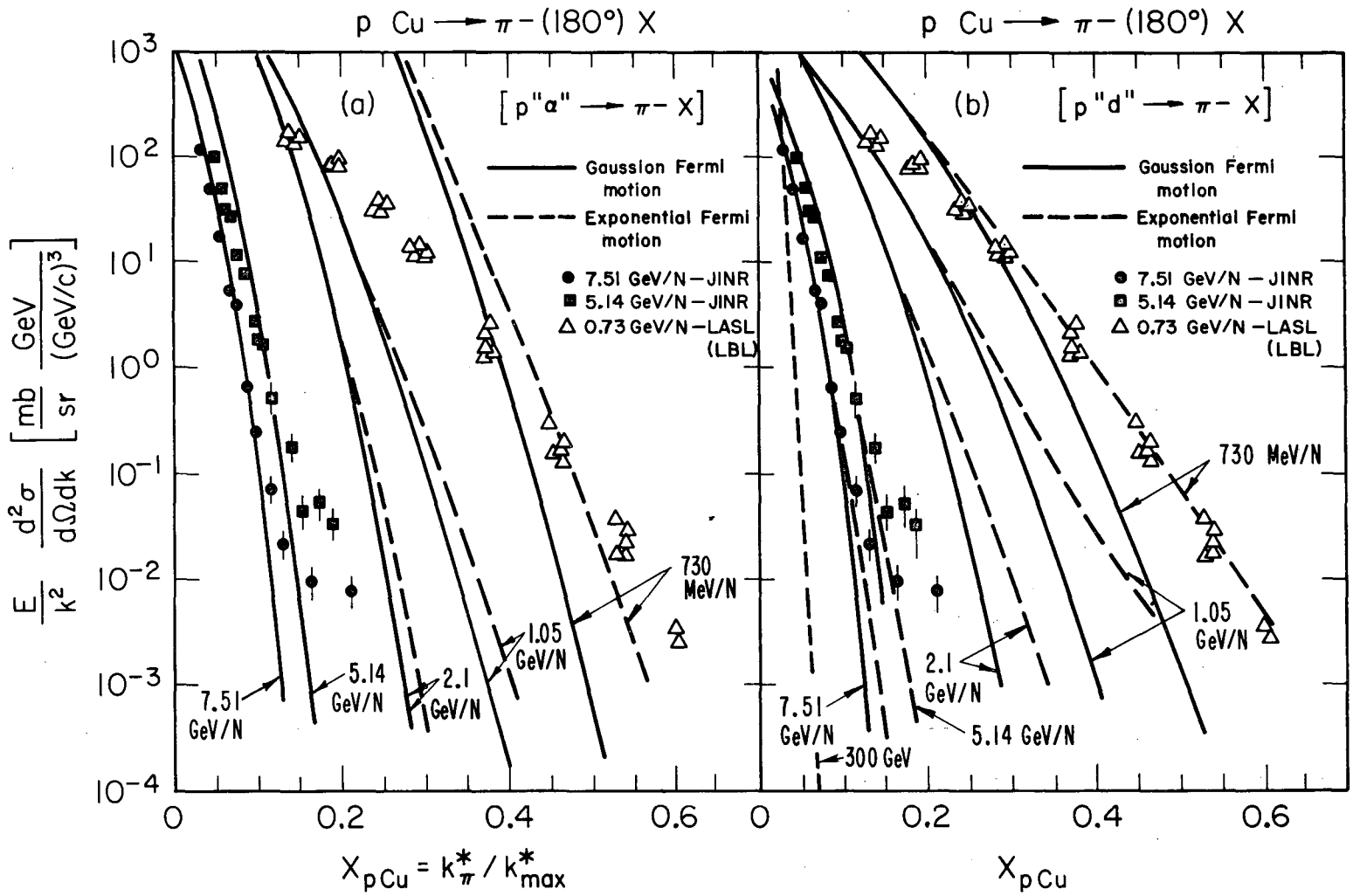

XBL 784−687

Fig. VII

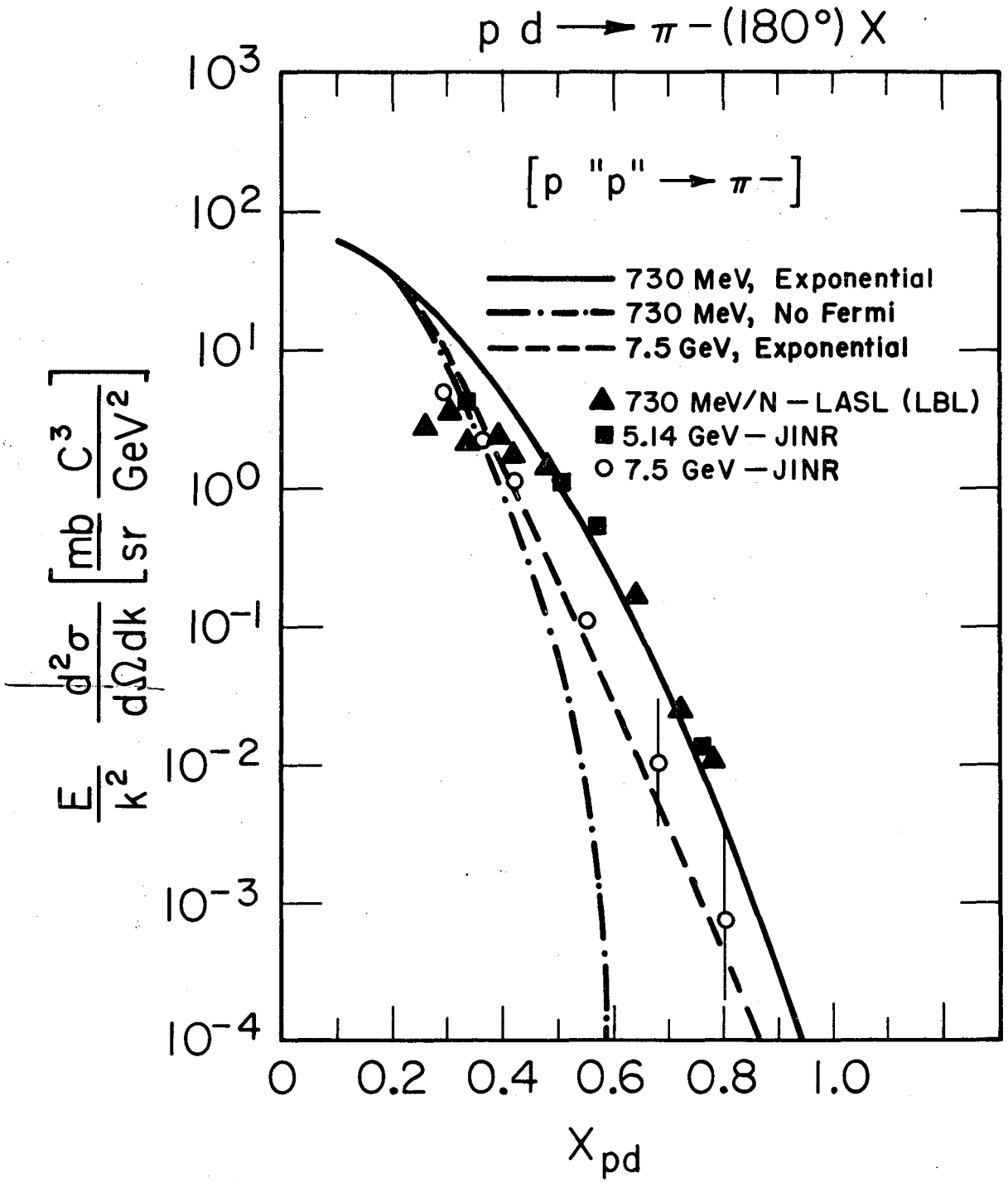

Fig. VIII XBL 784-683

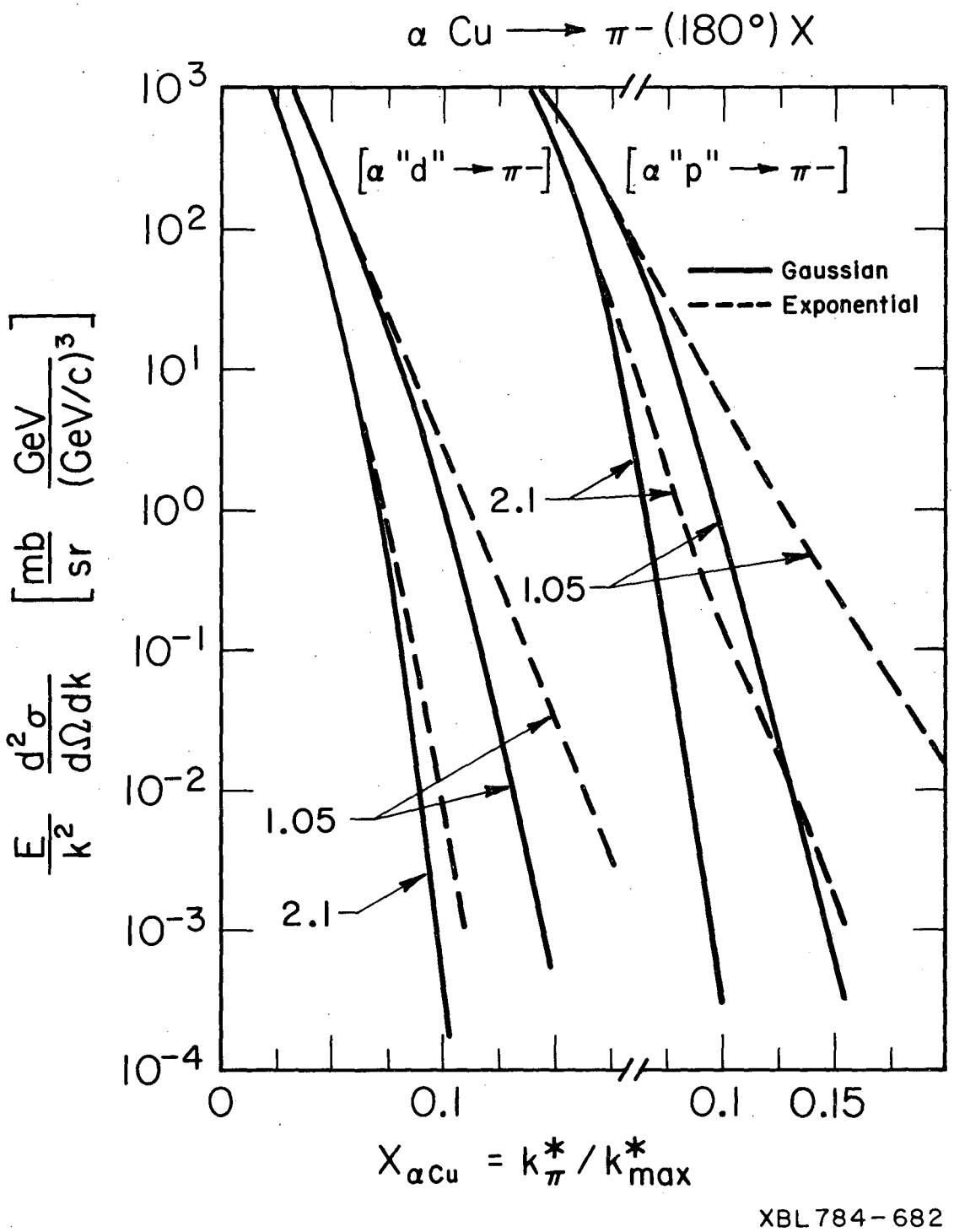
α Cu ⟶ π⁻(180°) X
[α "d" ⟶ π⁻]
[α "p" ⟶ π⁻]
Gaussian
Exponential
2.1
1.05
1.05
2.1
$\frac{E}{k^2}\frac{d^2\sigma}{d\Omega dk}\left[\frac{mb}{sr}\frac{GeV}{(GeV/c)^3}\right]$
10^3
10^2
10^1
10^0
10^{-1}
10^{-2}
10^{-3}
10^{-4}
0
0.1
0.1
0.15
$X_{\alpha Cu} = k^*_\pi / k^*_{max}$
XBL 784-682

Fig. IX

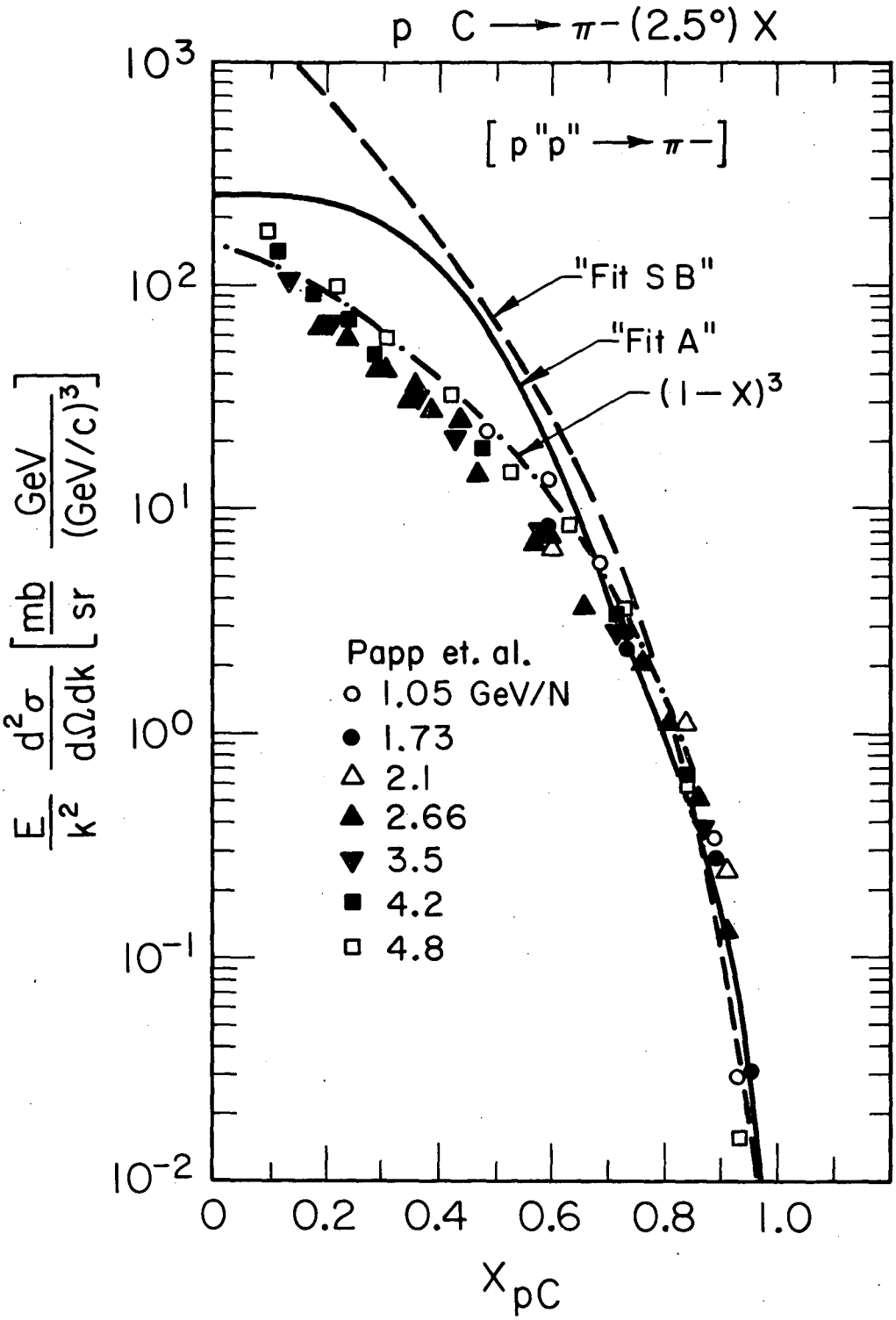

Fig. X

XBL 784-685

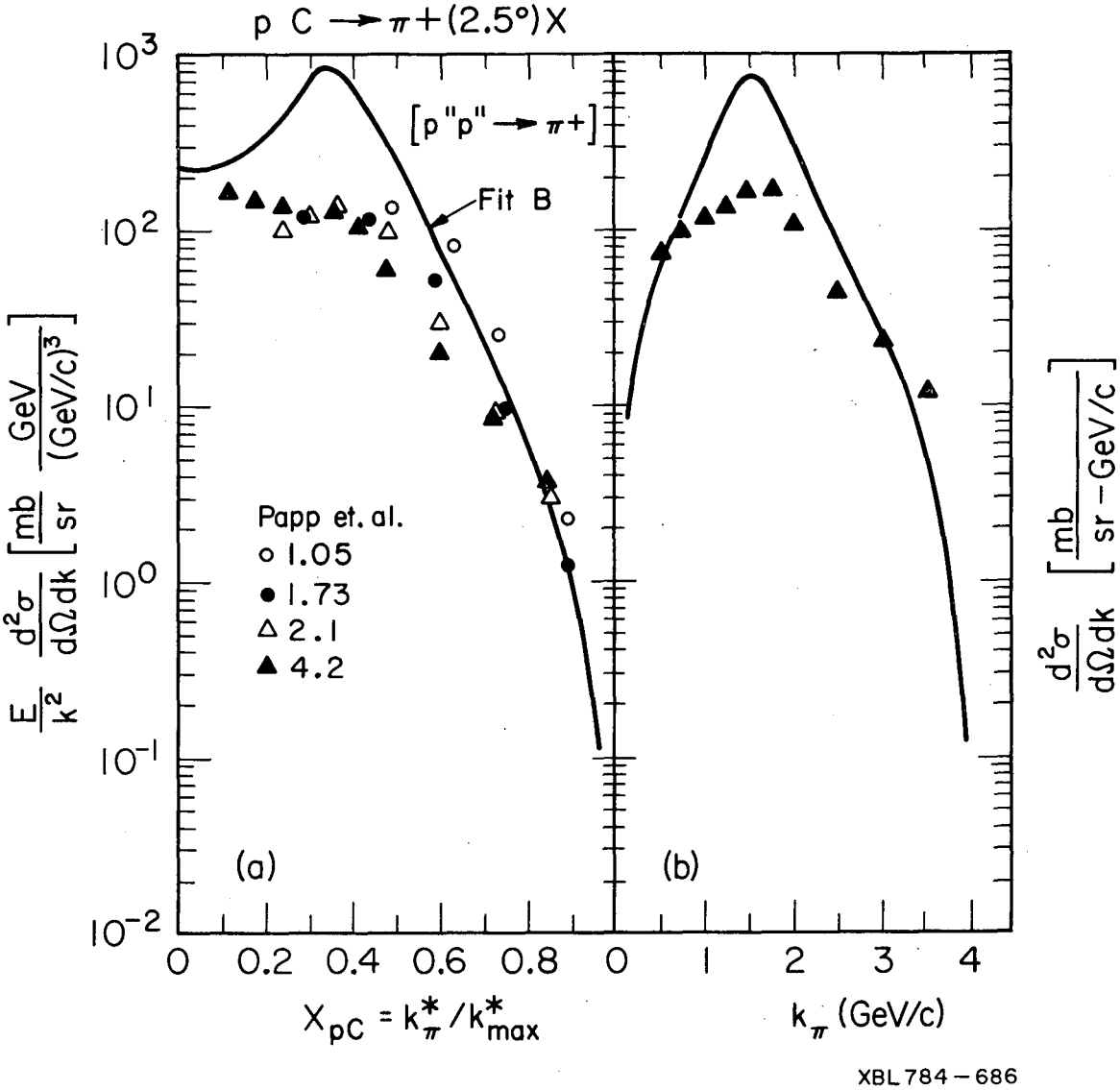
p C → π+(2.5°)X
[p"p" → π+]
Fit B
Papp et. al.
○ 1.05
● 1.73
△ 2.1
▲ 4.2
(a)
(b)
$\frac{E}{k^2}\frac{d^2\sigma}{d\Omega dk}\left[\frac{mb}{sr}\frac{GeV}{(GeV/c)^3}\right]$
$\frac{d^2\sigma}{d\Omega dk}\left[\frac{mb}{sr-GeV/c}\right]$
$X_{pC} = k^*_\pi / k^*_{max}$
k_π (GeV/c)
XBL784-686

Fig. XI

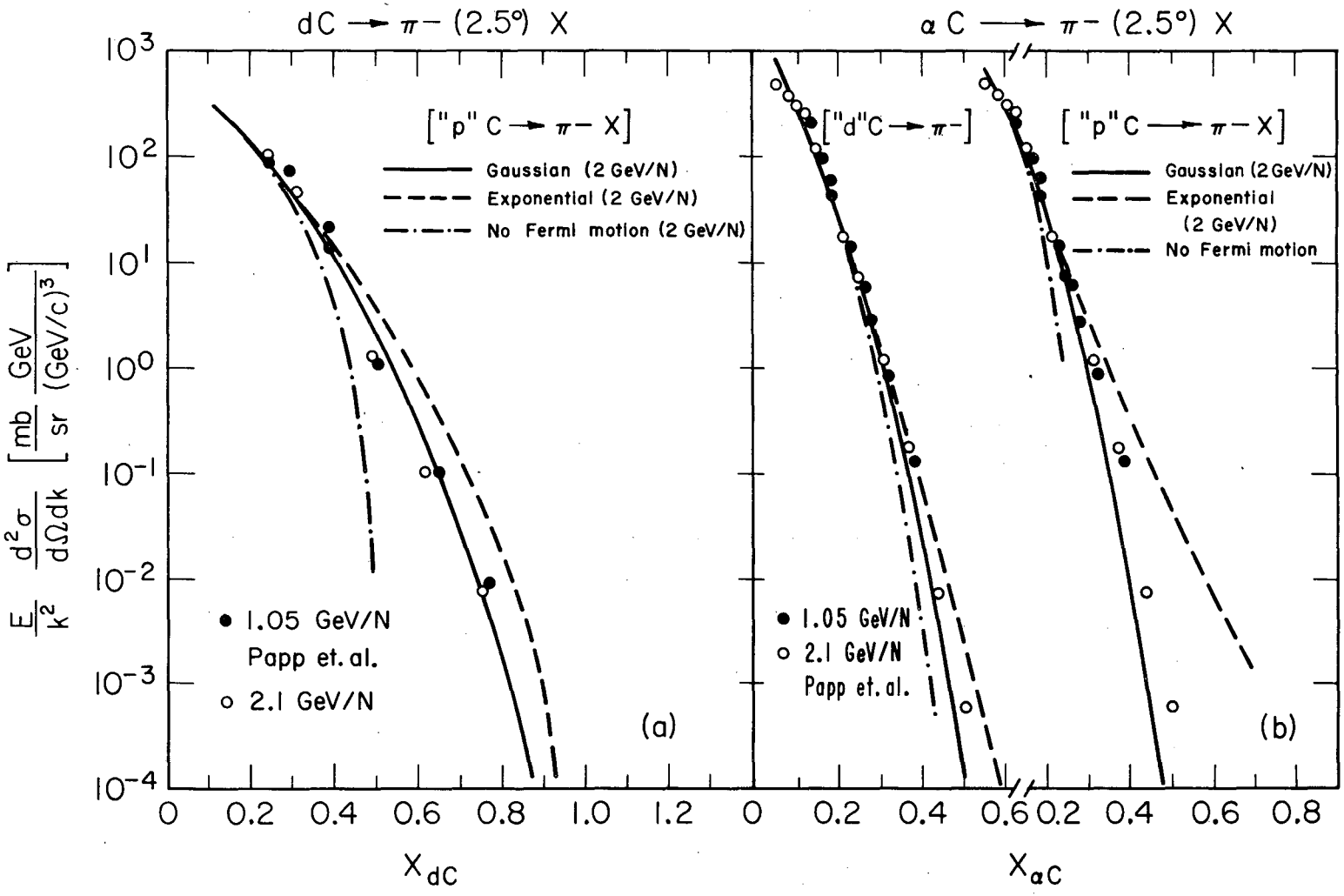

Fig. XII

XBL 784-8256

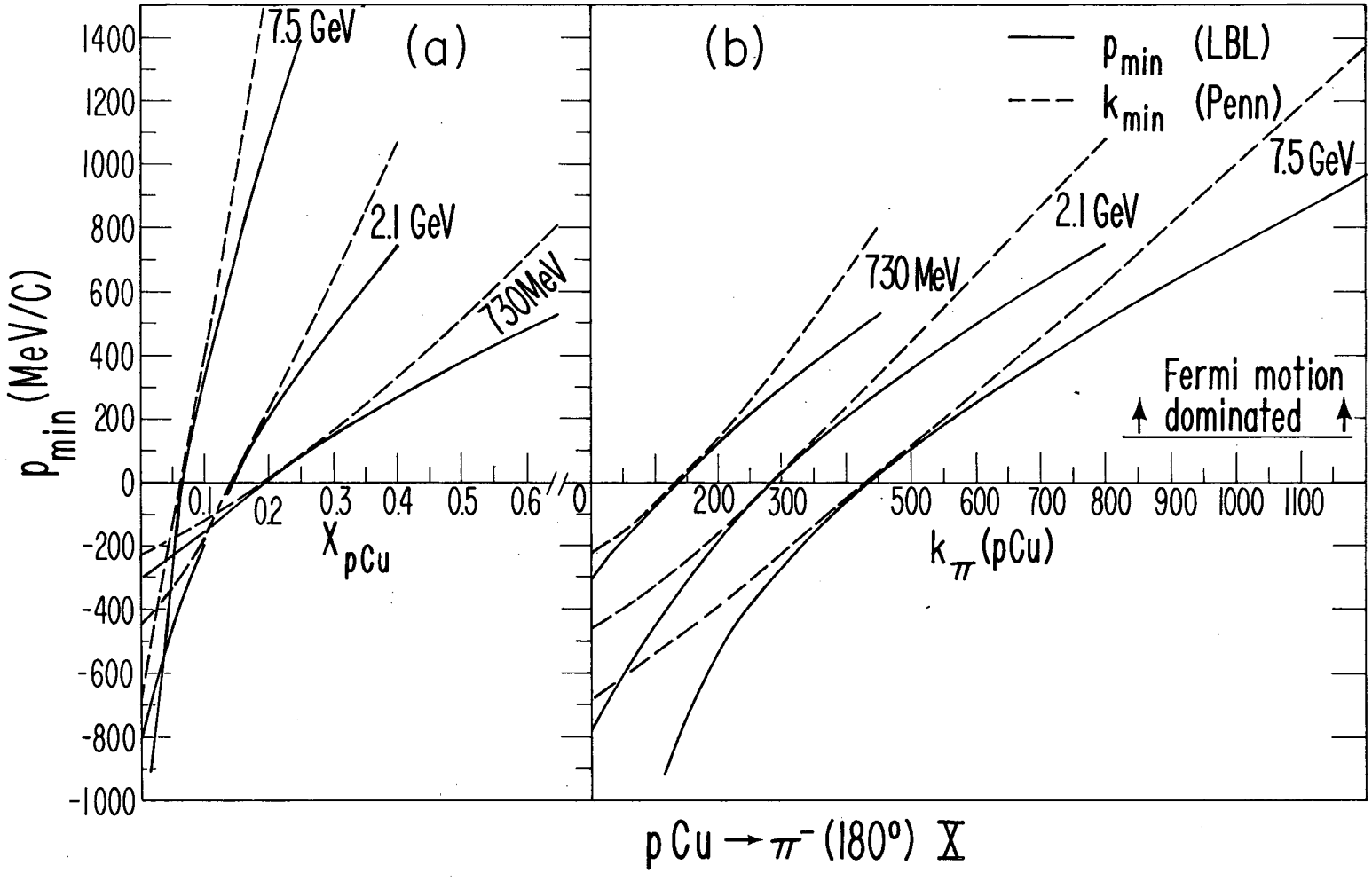
(a)
(b)
7.5 GeV
2.1 GeV
730MeV
p_{min} (LBL)
k_{min} (Penn)
Fermi motion dominated
p_{min} (MeV/C)
X_{pCu}
k_{π} (pCu)
p Cu → π⁻ (180°) X
XBL784-2501

Fig. XIII

This report was done with support from the Department of Energy. Any conclusions or opinions expressed in this report represent solely those of the author(s) and not necessarily those of The Regents of the University of California, the Lawrence Berkeley Laboratory or the Department of Energy.

TECHNICAL INFORMATION DEPARTMENT
LAWRENCE BERKELEY LABORATORY
UNIVERSITY OF CALIFORNIA
BERKELEY, CALIFORNIA 94720